NASA/TM-2005-XXXXXX

Report on Ocean Color and Carbon Study for the South Atlantic Bight and Chesapeake Bay Regions

Sergio R. Signorini, Charles R. McClain, Antonio Mannino, and Sean Bailey
Goddard Space Flight Center, Greenbelt, MD

Acknowledgements

This work was supported under a NASA Research Announcement 03-OES-03, Interdisciplinary Science in the NASA Earth Science Enterprise. The proposal title is "Eastern U.S. Continental Shelf Carbon Budget Modeling, Data Assimilation, and Analysis", Eileen Hofmann, Principal Investigator. We are thankful to Jay O'Reilly for providing guidance on the processing and mapping of the NOAA Coast Watch AVHRR SST data sets for the South Atlantic Bight region. We also acknowledge the help from Bryan Franz on the modification of the MSl12 code to include the GSM01-CB and POC algorithms, and Jeremy Werdell for useful guidance on the use of SeaBASS and NOMAD data archives. Finally, we are thankful to Larry Harding, Mike Mallonee, Mike Behrenfeld, Jim Yoder, and Jay O'Reilly for their inputs to the primary productivity, chlorophyll-a, and POC analyses.

PROLOGUE

This TM summarizes the results of ocean color algorithms applications and analyses of biomass and carbon data sets for the South Atlantic Bight (SAB) and Chesapeake Bay regions. This study is part of a larger multi-disciplinary, multi-institutional effort to study the Eastern U.S. Continental Shelf carbon budget (U.S. Eastern Continental Shelf Carbon Budget: Modeling, Data Assimilation, and Analysis, U.S. ECoS), a project funded by the NASA Earth System Enterprise Interdisciplinary Science Program that started in the summer 2004. Here we provide algorithm testing and intercomparison for chlorophyll-a (*Chl-a*), particulate organic carbon (POC), dissolved organic carbon (DOC), and primary production (PP) for the SAB and Chesapeake Bay (*Chl-a* and DOC only). A review of the physical and biogeochemical processes that drive the observed variability of oceanographic properties in the SAB (Section 2) is provided and the study results are related to those processes. Section 3 provides an analysis of several *Chl-a* algorithms for the SAB and Chesapeake Bay. In Section 4 we discuss the long-term variability (SeaWiFS period of September 1997 – April 2004) of *Chl-a* and POC based on ocean color retrievals in the SAB. In Section 5 we provide an analysis of PP data in the SAB and consequences on the validation and application of ocean color PP algorithms. Section 6 presents a summary of the pCO_2 variability and carbon balance study of *Cai et al.* [2003] based on a cross-shelf transect in the central SAB. Section 7 provides an analysis of chromophoric dissolved organic matter (CDOM) and DOC for the Chesapeake Bay using *in situ* and ocean color data. Finally, in Appendix A we provide a description of all algorithms used in this study, while Appendix B provides the validation steps of the standard protocol for satellite versus *in situ* data match-ups.

1. Summary of the SAB Ocean Processes

A brief summary of the SAB ocean processes is offered in this section to provide a background on the mechanisms that may influence algorithm performance and the analysis of available data sets. This summary is based mainly on information provided in the U. S. Department of Energy (DOE) report on SAB ocean processes [*Menzel*, 1993], which provides an excellent description of the SAB ocean processes based on DOE-sponsored cruises and the rich literature available at that time. Numerous papers have also been published on the SAB biological processes based on ocean color satellite data [*Blanton et al.*, 1984; *Bontempi and Yoder*, 2004; *Ishizaka*, 1990a; *Ishizaka*, 1990b; *Ishizaka*, 1990c; *McClain and Atkinson*, 1985; *McClain et al.*, 1990; *McClain et al.*, 1984; *McClain et al.*, 1988; *Yoder et al.*, 1981b; *Yoder et al.*, 1987]. The continental shelf of the SAB is regionally divided by the bathymetry (Figure 1) as inner shelf (0–20m), middle shelf (20–40m), and outer shelf (40–60m). The middle and outer shelves share similar ocean processes and therefore have been combined into a single group. An estimate of the coastal carbon budget [*Cai et al.*, 2003] for the SAB shelf is also provided.

- **Inner Shelf (0-20m)**
  - Multi-inlet coastline connecting low-lying coastal marshes to the ocean.
  - Circulation influenced by river discharge, tides, and winds.
  - Tidal transport and mixing provides two-way exchange of materials between estuaries and the ocean. In some cases the ocean is the source of materials accumulated in the estuaries.
  - *Chl-a* concentrations range from 1 to 25 mg m^{-3} and reflect a decreasing abundance of phytoplankton in the seaward direction.
  - Production is driven primarily by the rates at which nutrients are recycled and/or re-suspended from the sediments.
- **Middle and Outer Shelves (20-40m and 40m-60m)**
  - Circulation highly variable due to combined influence of tides, winds, and Gulf Stream intrusions. Subsurface intrusions of NACW occur mostly from May to August.
  - More event-scale variability in plankton abundance and production than in the inner shelf. Plankton densities may change 10-fold or more within days.
  - Flow convergence near the Charleston Bump is the preferred means of offshore export of carbon.
- **Carbon Exchange between Atmosphere, Land-Shelf Interface, and the Ocean**
  - The coastal carbon budget, based on data from Wassaw sound and the adjacent SAB continental shelf, was analyzed by *Cai et al.* [2003]. This analysis revealed that marshes and estuaries are sinks of atmospheric carbon (7.1×10^{12} gC yr^{-1}) and sources of DIC (1.3×10^{12} gC yr^{-1}) and OC (6.0×10^{12} gC yr^{-1}), while the SAB shelf region acts as a source of CO_2 to the atmosphere (2.7×10^{12} gC yr^{-1}) and exports DIC (1.3×10^{12} gC yr^{-1}), and possibly OC (2.0×10^{12} gC yr^{-1}), to the deep ocean.

2. Chlorophyll-a Algorithms for the SAB and Chesapeake Bay (CB)

Four *Chl-a* algorithms (OC4v4, Clark, Carder, GSM01) were tested in the SAB and five in the CB (OC4v4, Clark, GSM01, GSM01-CB, and Carder). A detailed description of these algorithms is provided in Appendix A. Match-ups between SeaWiFS *Chl-a* retrievals and *in situ* near-surface *Chl-a* from the SeaWiFS Bio-optical Archive and Storage System (SeaBASS) were conducted following standard protocols [*Hooker*, 2000; *McClain et al.*, 2000; *McClain et al.*, 1982; *Werdell and Bailey*, 2002; *Werdell et al.*, 2003]. Figure 2 shows the individual algorithm match-ups for the SAB in the form of scatter plots. All four algorithms performed well (r^2>0.8), with the OC4v4 having the least absolute percent difference (APD=47%). However, there are some distinctions to be made between the empirical (OC4v4, Clark) and the semi-analytical (GSM01, Carder) algorithms. Figure 3 illustrates some of these distinctions. One major distinction is that empirical algorithms are more stable, especially the OC4v4 which provides band ratio choices to avoid the use of unrealistically low or negative retrievals in the blue bands.

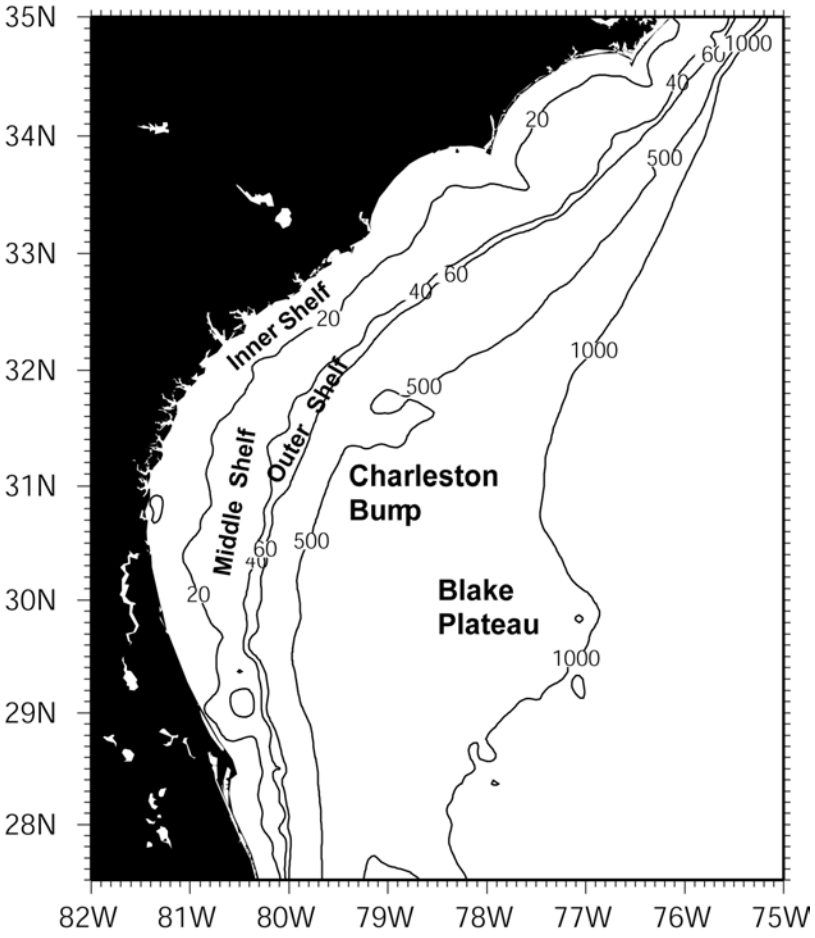

Figure 1. Map of the South Atlantic Bight showing the bathymetry limited regional shelf domains.

The semi-analytical algorithms, by their nature (see Appendix A), utilize all available bands and are therefore more affected by unrealistic retrievals in the blue bands. An example of that is

the GSM01 negative retrievals (black patch near the coast in Figure 3c) near shore, most likely due to large concentrations of CDOM originating from elevated river discharge in spring (May 24 2000), which significantly reduces the signal in the blue bands. The Carder algorithm retrieves reasonable *Chl-a* values in the CDOM plume (Figure 3d) because it defaults to an empirical algorithm in such conditions. However, the transition between the semi-analytical and empirical *Chl-a* retrievals is not entirely smooth as seen from the dark blue line separating the high *Chl-a* coastal plume from the much lower *Chl-a* concentrations offshore. However, semi-analytical algorithms are capable of retrieving inherent optical properties (IOPs) in addition to *Chl-a*, e.g., CDOM absorption and backscatter coefficients, which are indispensable for a variety of applications. Some examples are DOC algorithm development and evaluation of phytoplankton growth from space based on backscatter (see Sections 5, 7 and Appendix A). Therefore, further studies should be done with semi-analytical algorithms, especially in turbid waters of the coastal ocean, to improve our understanding of interactions between phytoplankton biomass/growth and dissolved and suspended materials in the water column.

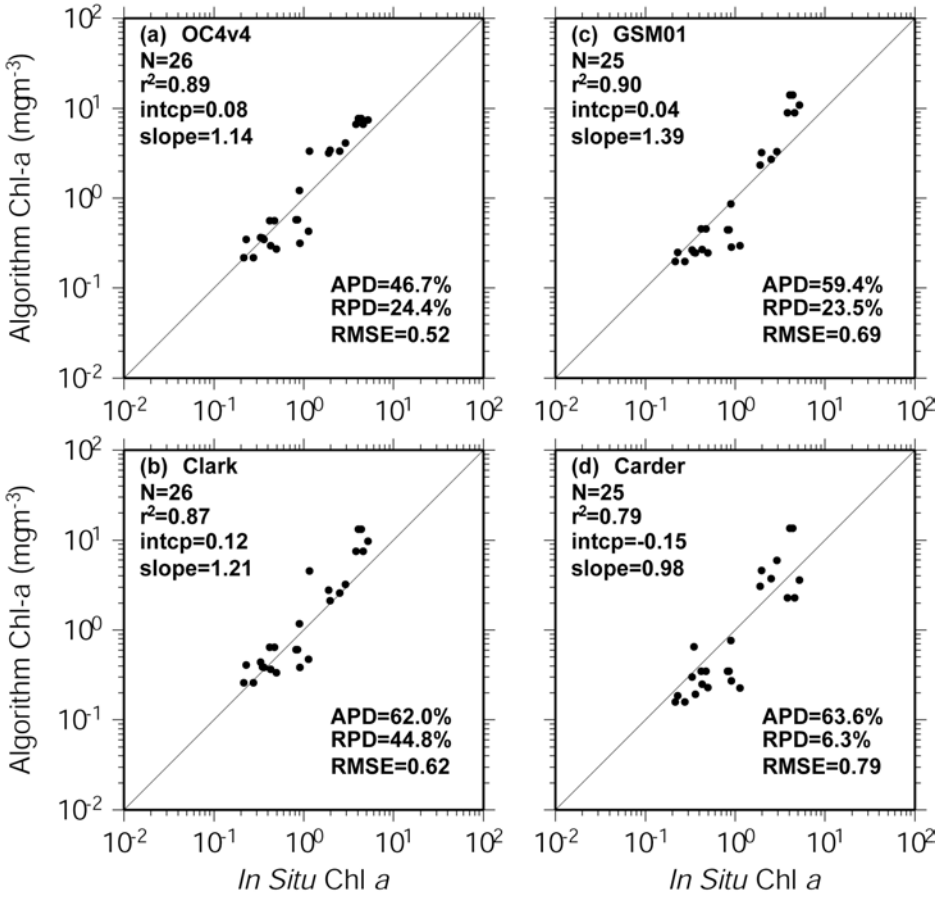

Figure 2. SeaWiFS *Chl-a* match-ups using four different algorithms: OC4v4, GSM01, Clark, and Carder.

Figure 4 shows *Chl-a* composites for April – September 2003 derived from SeaWiFS L2 reflectances and 5 different algorithms, OC4v4, Clark, Carder, Garver-Siegel-Maritorena 2001 (GSM01) [*Garver and Siegel*, 1997; *Maritorena et al.*, 2002], and a regionally-tuned version [*Magnuson et al.*, 2004] of GSM01 (GSM01-CB). The square/crosses indicate the locations

where there are available match-ups (observed and satellite) during the SeaWiFS period (September 1997 – December 2004). No match-ups are available for the GSM01-CB because the algorithm is not online on the SeaWiFS project system to conduct match-ups with the standard protocol. A modified version of the code was used instead on a desktop computer to obtain the GSM01-CB *Chl-a* retrievals. However, the GSM01-CB and Carder algorithms are compared for the same locations used for the match-up analysis. The statistical results for OC4v4, Clark, GSM01, and Carder algorithms are summarized in the scatter plots. The means and STDs at the match-up points for the observed values, and OC4v4, Clark, GSM01, and Clark algorithms are 7.55/5.77, 7.00/4.88, 5.25/5.66, 4.56/5.30, and 7.96/6.90, respectively. The Carder algorithm has the highest correlation (r^2=0.81) with the *in situ* data. The GSM01 is biased low, primarily at higher (>2 mg/m^3) *Chl-a* values. However, the GSM01-CB retrieves values that compare well with the other algorithms. For example, the means and STDs for the Carder and GSM01-CB based on the April – September 2003 composites, at the match-up locations are 20.60/6.83 and 23.81/8.32, respectively. An "off-line" match-up analysis (Appendix B) was conducted with the stand-alone code for the Chesapeake Bay region using OC4v4, GSM01, and GSM01-CB algorithms. Both *in situ* and satellite reflectances were used for the match-ups. The results indicate that the GSM01-CB (regionally tuned) algorithm provides the best statistical fit to the data.

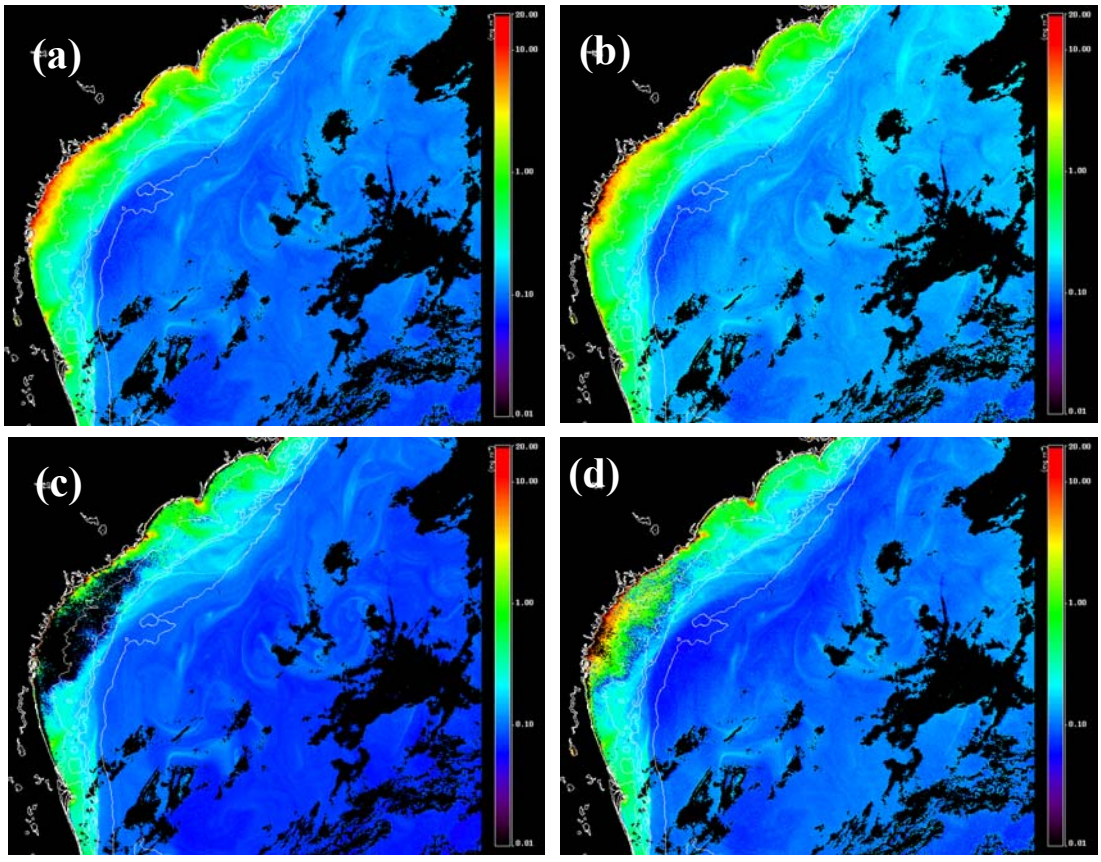

Figure 3. SeaWiFS *Chl-a* images for May 24, 2000 using four algorithms: (a) OC4v4, (b) Clark, (c) GSM-01, and (d) Carder. Note in (c) and (d) that both semi-analytical algorithms are affected by the elevated CDOM concentrations originating from river discharge.

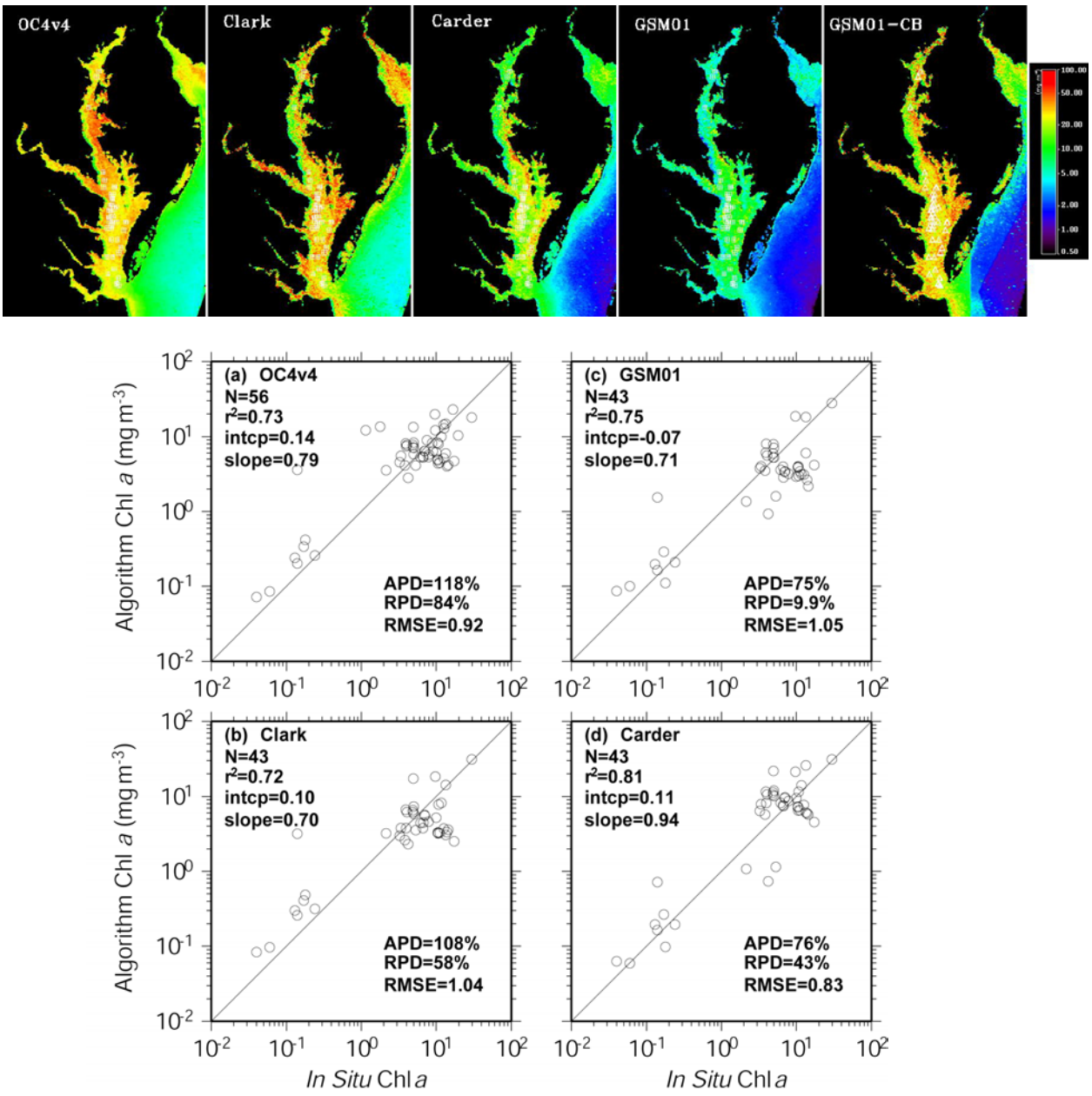

Figure 4. Top panel: chlorophyll (0.5 – 100 mg m^{-3}) composites for April-September 2003 derived from SeaWiFS L2 reflectances and 5 different algorithms, OC4v4, Clark, Carder, Garver-Siegel-Maritorena 2001 (GSM01) [*Garver and Siegel*, 1997; *Maritorena et al.*, 2002], and a regionally-tuned version [*Magnuson et al.*, 2004] of GSM01 (GSM01-CB). The square/crosses indicate the locations where there are available match-ups (observed and satellite) during the SeaWiFS period (September 1997 – December 04). Bottom panel: match-up scatter plots for the OC4v4, GSM01, Clark, and Carder algorithms.

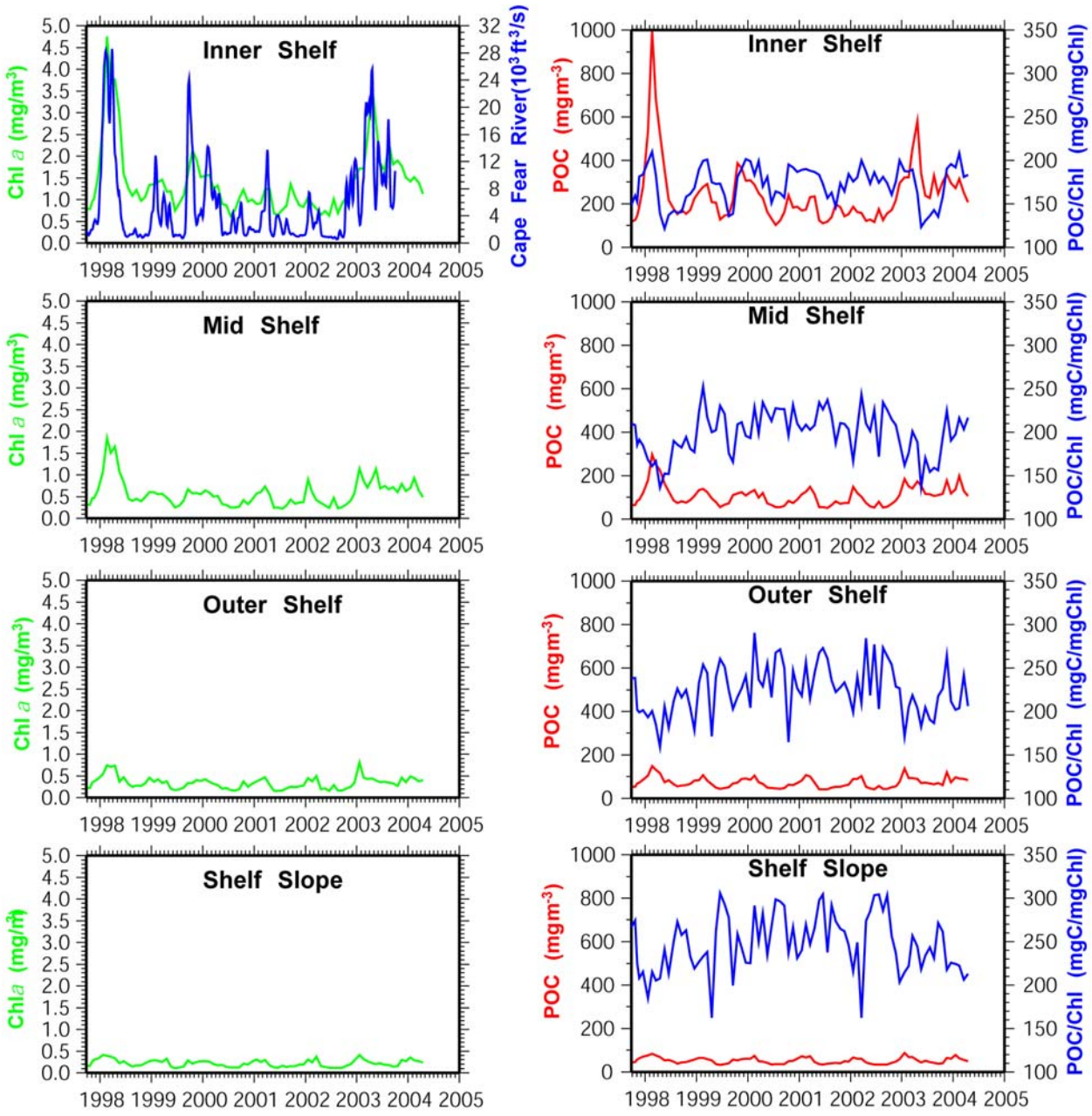

Figure 5. Time series of chlorophyll and POC for each SAB regional shelf domain.

3. SAB Chlorophyll and POC Time Series

Time series of *Chl-a* and POC were produced based on water-leaving radiances (nLws) from SeaWiFS L2 SAB cutouts and OC4v4 (*Chl-a*) and Clark (POC) algorithms. The time series cover the period of September 1997 – April 2004, the SeaWiFS data available at the time of processing. Regional *Chl-a* and POC averages were calculated for the inner-, middle-, outer-shelves and slope regions. The time series are shown in Figure 5. The Cape Fear River monthly mean discharge is superposed on the inner shelf *Chl-a* time series and the POC:*Chl-a* ratios for

each region are superposed on the correspondent POC time series. The largest river discharges occurred during the spring of 1998 and 2003, following El-Niño events. The increase in river discharge is manifested as an increase in both *Chl-a* and POC concentrations, most probably due to carbon and nutrient enhancement from river sources.

Figure 5 also shows a seaward decrease (from the inner shelf to the slope) in *Chl-a* and POC concentrations, whereas the POC:*Chl-a* ratio increases seaward. This result indicates that the *Chl-a* concentration decreases more rapidly than the POC towards the open ocean and reaches a maximum value in Gulf Stream waters near the shelf slope. Both *Chl-a* and POC exhibit seasonal cycles, with a maximum in spring and a minimum in summer.

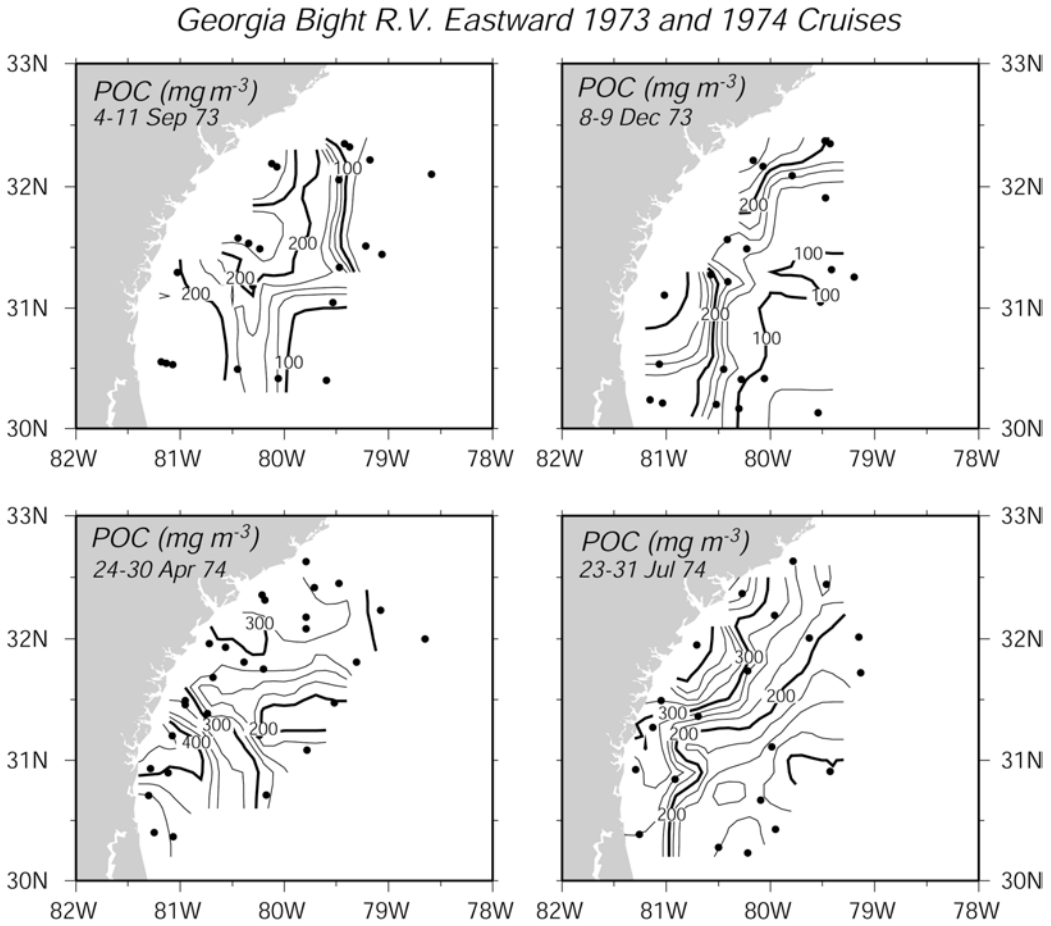

Figure 6. Surface distribution of POC from 4 cruises in the Georgia Bight (GAB73-74).

Table1. Satellite derived POC for April, July, September, and December of 1998 through 2003, and surface POC from GAB73-74 cruises of September 1973, December 1973, April 1974, and July 1974. Units are in mg C/m^3. Two multi-year satellite means are shown, one for 1998-2003 and another for 1999-2002 (without El-Niño years).

Year	**1973**	**1974**	**1998**	**1999**	**2000**	**2001**	**2002**	**2003**	**98-03**	**99-02**
Apr		327	745	322	380	395	189	974	501	321
Jul		236	329	249	153	260	273	302	261	233
Sep	157		117	153	138	180	160	170	153	157
Dec	167		195	181	113	135	204	187	169	159

Figure 6 shows the surface distribution of POC in the Georgia Bight obtained from data collected in September 73, December 73, April 74, and July 74. Monthly POC averages derived with the Clark algorithm and SeaWiFS nLws for the same months of 1998 through 2003 are summarized in Table1. The monthly satellite-derived POC values were derived from pixels surrounding (20-km window) the station locations. Note that the April 1998 (745 mg/m3) and the April 2003 (974 mg/m3) are the largest among the monthly means due to the increased river discharge during those years. The overall satellite monthly means for April become much closer if 1998 and 2003 are removed from the mean. There is very good overall agreement for all 4 months (less than 2%). However, these results must be taken with caution since the observations are not concurrent with the satellite data and significant year-to-year variability is present.

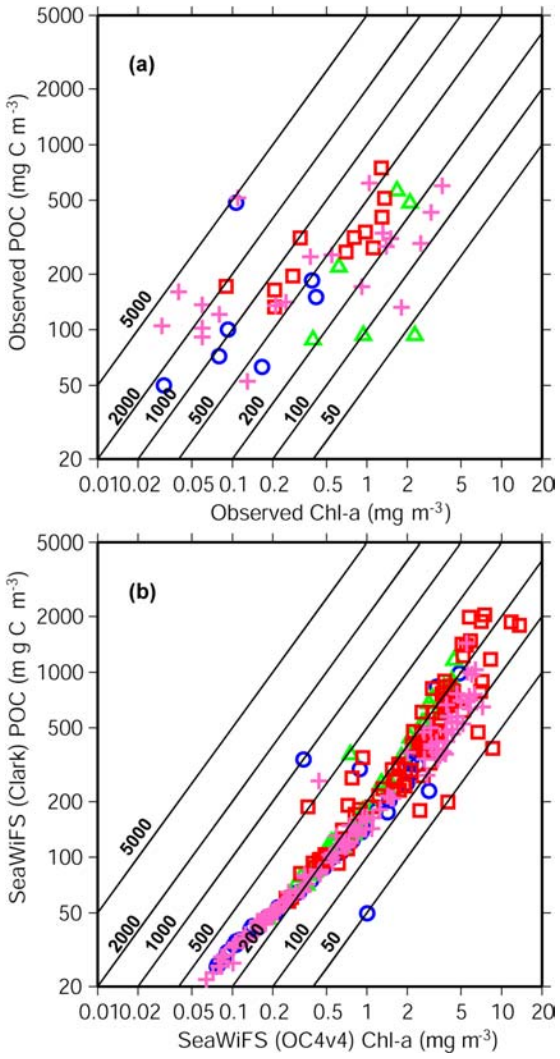

Figure 7. Scatter plots of POC versus *Chl-a*: (a) observed POC versus observed *Chl-a* from GAB73-74 cruises; (b) SeaWiFS-derived POC (Clark) versus *Chl-a* (OC4v4). The lines of equal POC:*Chl-a* ratio (50 – 5000) are superposed on both scatter plots. The symbols are for September (blue circles), December (green triangles), April (red squares), and July (purple crosses) cruises and SeaWiFS monthly composites.

The POC:*Chl-a* ratios from the GAB73-74 cruises (September 73, December 73, April

74, and July 74) and those derived from SeaWiFS data are given in Figure 7. The SeaWiFS-derived POC (Clark) and *Chl-a* (OC4v4) were obtained from monthly composites corresponding to the cruise months (April, July, September, and December 97-04) and at the station locations with an averaging window of 4x4 km. Again, since the GAB73-74 data are not contemporaneous with SeaWiFS coverage, the comparison must be analyzed with caution. However, some differences between observed and satellite-derived data are quite obvious. Some of these differences may be due to the large interannual variability in river discharge. The range of satellite POC values is much larger than the observed range (20 – 2000 versus 50 – 750, respectively). The satellite-derived POC:*Chl-a* ratios (50 – 1000) are much less variable than those derived from the *in situ* data (50 – 5000). More recent *in situ* data (1985-1988) indicate much smaller ranges of POC:*Chl-a* ratios (132–332) for the SAB inner shelf in the vicinity of Wassaw Sound [*Verity et al.*, 1993]. These differences can only be reconciled when concurrent satellite and in situ data become available for the SAB. There are some satellite-derived *Chl-a* values higher than 5 mg m^{-3} that are not present in the in situ data. This is not surprising since all *Chl-a* algorithms tested in the SAB tend to overestimate *Chl-a* for values above 3 mg m^{-3} (see Figure 2).

Contemporaneous particulate carbon (PC) *in situ* data are available for match-up analysis in Chesapeake Bay. Strictly speaking, the PC data would include particulate inorganic carbon (PIC) as well. However, the PIC concentrations in Chesapeake Bay are extremely low or non-existent (A. Mannino personal communication). Therefore, using *in situ* PC in lieu of POC for the Chesapeake Bay match-up analysis is a very good approximation. The results are given in Appendix B. Two algorithms were used, Stramski-4 and Clark (see Appendix A for algorithm description). The Clark algorithm was applied using both in-band and full-band water-leaving radiances but the differences in the results are very subtle. The Stramski-4 algorithm, since it was not developed for coastal waters, has a tendency to saturate at high POC values (>1000 mg m^{-3}) and therefore is biased low. The Clark algorithm provides much less biased retrievals, albeit with r^2 typically less than 0.1. However, the correlation coefficient would significantly increase if a larger dynamic range of data values were available, especially in the low end of the data range (50 to 300 mg m^{-3}).

5. Analysis of Primary Production Data in the SAB and Consequences on the Validation and Application of Ocean Color PP Algorithms

5.1. Background

A time series of primary production for the SAB, derived from SeaWiFS *Chl-a*, PAR, and SST from NOAA Coastwatch AVHRR data, and the VGPM2 algorithm (a variation of the well-known VGPM [*Behrenfeld and Falkowski*, 1997] with Eppley's P_B^{opt}(SST)), was produced for the period of September 1997 – April 2004. The overall annual mean PP based on available SeaWiFS whole years at the time (1998 – 2003) was compared with annual PP estimates published in the DOE Report [*Menzel*, 1993] for three regions of the continental shelf: inner shelf (0-20m), middle shelf (20-40m), and outer shelf (40-60m). Values for the shelf slope (60-500m) were also tabulated but no equivalent in situ data are available for comparison. The results are summarized in Table 2.

Inspection of Table 1 shows that there is significant interannual variability in the satellite-derived PP and that the agreement with the DOE data varies from year to year, but since

the DOE values are based on data collected between 1979 and 1990, some of the differences may be attributed to interannual variability of nutrient availability in the euphotic layer. Considering that we are comparing PP estimates from different years, the overall agreement between in situ PP values and satellite-derived PP values is not unreasonable. However, this analysis ignores bottom illumination (~10 to 20% of surface PAR) on the shallow continental shelf, which is inconsistent with the VGPM. More specifically, the euphotic depth (Z_{eu}) can be much larger than the local depth, causing overestimates of PP since Z_{eu} is a multiplier factor in the VGPM algorithm. In view of this, the following analyses were conducted to find a possible strategy to adjust the VGPM algorithm to retrieve more accurate values on the shallow shelf, or to find an alternate methodology to obtain more accurate PP estimates from space.

Table 2. Rates of primary production (PP in gC m^{-2} yr^{-1}) for the SAB inner (0-20m), mid (20-40m), and outer (40-60m) shelves, and shelf slope (60-500m) regions. The observed (Obs) values are from the DOE Report. The yearly (1998-2003) and the the overall average (Avg) values are derived using the VGPM2 algorithm and satellite data. The DOE Report *in situ* estimates were derived from seasonal studies consisting of short-term measurements of ^{14}C uptake (*Yoder*, 1985; *Verity* et al., manuscript).

Region	**Obs**	**Avg**	**1998**	**1999**	**2000**	**2001**	**2002**	**2003**
Inner	620	446	635	486	410	324	262	660
Middle	248	278	404	296	245	197	167	402
Outer	360	211	285	228	195	155	136	282
Slope	…	161	212	181	154	119	105	197

5.2. Primary production i*n situ* data

Primary production data from 5 cruises were compiled and converted to electronic format from cruise reports and data logs. Four of these cruises were conducted in the Georgia Bight on the R. V. Eastward during September 1973 (E-13-73), December 1973 (E-19-73) , April 1974 (E-03-74), and July 1974 (E-12-74), hereafter referred to as GAB73-74. The stations were conducted from nearshore to beyond the shelf break. The fifth cruise was conducted within the coast and the 20-m isobath and was designed to evaluate the effects of precipitation on the inner shelf oceanography (Spring Removal Experiments, SPREX I and II). The SPREX cruises were designed to study cross-shelf exchange processes between Savannah, Ga., and Cape Romain, N.C., their effects on biological/chemical rate processes, and the distribution of materials during the spring transition from horizontal to vertical stratification and when prevailing winds are from the south. There were more recent cruises conducted in the Georgia Bight. The Georgia Bight Experiment (GABEX) was designed to study the effect of Gulf Stream/shelf water interaction on the Georgia/Florida shelf during seasons that shelf waters are vertically mixed (GABEX-I) and when stratified (GABEX-II). Figure 8 shows a map with the station locations that have available data for analyses in this TM.

The total number of sampled locations is 83, 60 during GAB73-74 and 23 during SPREX-II. As mentioned before, there were other cruises where carbon data were collected but not all of them had cruise reports available for compilation (for instance, data from GABEX-I and SPREX-I are not available). Data from GABEX-II, which focused on the effects of summer Gulf Stream intrusions during July and August 1981 when the middle shelf waters were

vertically stratified, will be discussed in subsection 4.5. The above data sets were used to evaluate algorithm performance.

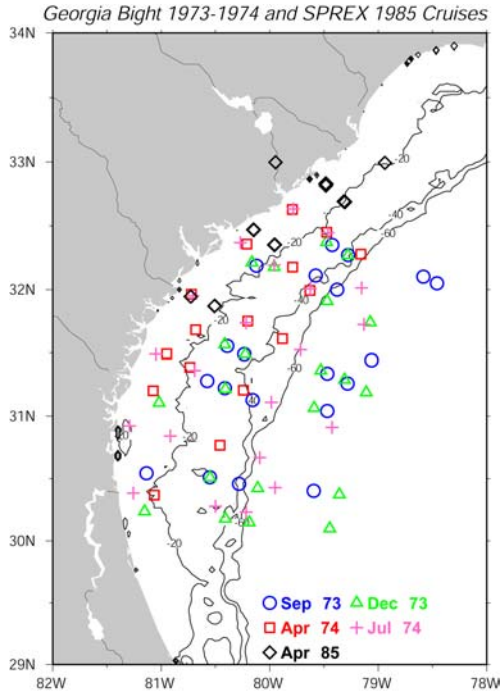

Figure 8. Station locations for the five Georgia Bight cruises for which primary production data are available.

5.3. Correction for Z_{eu} greater than local depth

As mentioned before, some areas of the inner and middle SAB shelf receive PAR illumination that may exceed 10% of the surface light intensity. This is better illustrated in Figure 9, which shows SeaWiFS monthly composites for May 1999 of *Chl-a*, diffuse attenuation coefficient at 490 nm (K_{490}), and percent of PAR that reaches the ocean floor based on two algorithms for K_{PAR}, one based on *Chl-a* [*Morel*, 1988] and one based on K_{490} [*J. Nelson*, unpublished]. The percent of light that reaches the bottom (PAR(H,%)) of the SAB shelf was computed using the SeaWiFS-derived K_{PAR} estimates and the exponential light attenuation equation. The equations for these calculations are:

$$K_{PAR} = 0.121C^{0.428} \tag{1}$$

$$K_{PAR} = 0.0304 + 0.893K_{490} \tag{2}$$

$$\mathrm{PAR}(H,\%) = 100\exp\left[-K_{PAR}H\right] \tag{3}$$

Figure 9 shows that the PAR(H,%) using the two different algorithms are very similar. The PAR(H,%) using the *Morel* K_{PAR} are 28.2%, 7.7%, and 4.3% for the inner, middle, and outer shelves. The equivalent percentages using the *Nelson* K_{PAR} are 27.3%, 6.7%, and 2.8%. These

large values of PAR at the bottom pose a challenge for ocean color algorithms since there is no account for Z_{eu} exceeding the local depth. Bottom reflection, especially in shallow/clear coastal waters, is another error source that can potentially bias the retrieval of satellite products. This is clearly seen near the coast of southern Florida (Figure 9) where the water depth is less than 5 meters and more than 80% of the surface PAR reaches the bottom. This is a difficult effect to correct or quantify but, assuming a perfect bottom reflector, then the same light attenuation is experienced coming back up. So, if 80% of surface PAR reaches the bottom, then about 64% would be reflected back up through the surface. However, the problem of Z_{eu} truncation due to large PAR values on the ocean bottom is a more tractable and will be addressed next. In an attempt to correct this problem, a simple formulation, based on the exponential light attenuation equation, was derived. Thus, for situations on the shallow shelf where Z_{eu} is greater than the local depth (D), the following correction equations were derived:

$$PP(D) = PP(Z_{eu}) [1 - \exp(-4.61D/Z_{eu})]/0.99 \quad (4)$$

or,

$$PP(D) = PP(Z_{eu}) [1 - \exp(-K_{PAR})]/0.99 \quad (5)$$

where PP(D) is the adjusted PP for depth D and $PP(Z_{eu})$ is the PP "seen" by the satellite. Table 3 shows a comparison between the uncorrected/corrected VGPM2 PP and the observed PP. The VGPM2 estimates were obtained using the observed SST, *Chl-a*, and PAR as input parameters. Z_{eu} was calculated from *Chl-a* using [*Morel and Berthon*, 1989]. There were no direct PAR measurements available from the GAB73-74 cruises, only cloud cover. Surface PAR for cloudy skies was obtained using the *Frouin et al.* [1989] method for clear skies PAR and the *Dobson and Smith* [1988] cloud algorithm.

Table 3 shows that the agreement between observed and estimated PP is not very good, except for September 73 and April 85 for which the observed and adjusted model estimates are within a difference of 6 to 7%. All the other values are either large underestimates or overestimates. Also, the observed PP has a strong seasonality with a peak in December and the smallest PP in July. In addition, there is indication of large interannual variability. The April 85 PP (309) is almost three times larger than the PP during Apr 74 (116). This large interannual variability may be related to differences in river runoff. USGS data show that the Cape Fear River discharge during April 1974 averaged 4122 cu ft/s, while the average discharge was only 970 cu ft/s (about 4 times less) during April 1985. It is known that the turbidity caused by river discharge can significantly reduced light penetration on the inner shelf causing a reduction in PP [*Yoder*, 1985]. Consequently, increases in nutrient fluxes are offset by the decrease in illumination. This may explain the differences in PP between April 1974 and April 1985.

The large PP seasonality is not captured by VGPM2. In fact, the VGPM2 production is larger for April and July 74 than for September and December 73. We will address the PP seasonality in the next section.

5.4. Primary production seasonality

Figure 10 shows a log-log plot of observed PP versus observed surface chlorophyll. The symbols identify the four GAB73-74 cruises. The dashed line represents the [*Eppley et al.*, 1985] algorithm. Only stations deeper than 20 meters were considered because they were less

influenced by the turbid waters originating from river discharge and sediment re-suspension. The SPREX-II data was not included because they were collected inshore of the 20-m isobath.

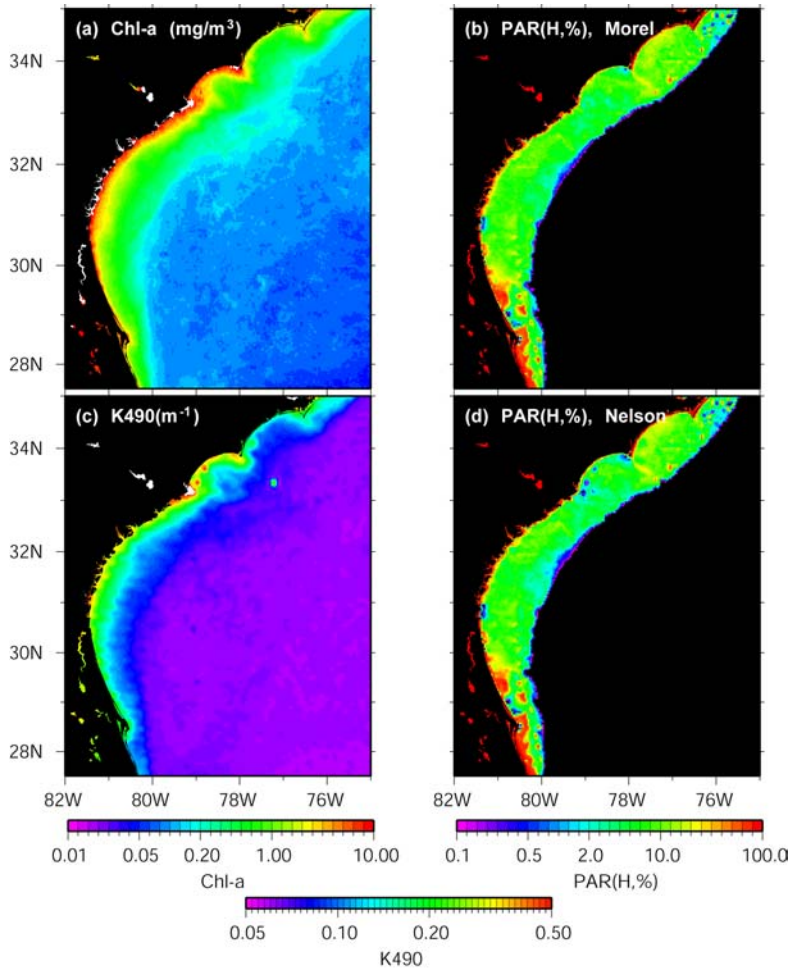

Figure 9. SeaWiFS-derived monthly composites of *Chl-a* (a), K_{490} (c), and percent of PAR that reaches the bottom of the continental shelf. PAR(H,%), based on the K_{PAR} algorithms of *Morel* (b) and *Nelson* (d).

There is a distinct difference between the September – December 1973 and the April – July 1974 linear fits (solid lines), indicating a strong seasonality in PP, but no significant change in chlorophyll concentrations. Evidence of considerable variability in primary production over daily to interannual scales, associated with relatively constant biomass, has been reported before in the SAB inner shelf waters [*Verity et al.*, 1993]. This suggests that production and consumption are coupled. This dynamic relationship is not unexpected in a system supported largely by regenerated nutrients [*Hanson et al.*, 1990].

The equation and seasonal coefficients for the log-log regressions (solid lines) shown in Figure 10 are:

$$PP(mgC/m^2/d) = 10\text{^}[a \log(Chl\text{-}a) + b] \quad (6)$$

Sep-Dec 73: a=0.8191, b=3.357, r^2=0.65
Apr-Jul 74 : a=0.7509, b=2.211, r^2=0.48
Eppley's : a=0.5000, b=3.000

Table 3. Comparison between observed (GAB73-74 and SPREX) and estimated (VGPM2) PP ($mgC/m^2/d$). The adjusted VGPM2 estimates (VGPM2A) are also tabulated.

Cruise	Obs. PP	VGPM2	VGPM2A
Sep 73	394	550	422
Dec 73	1288	632	582
Apr 74	116	866	730
Jul 74	100	1759	1591
Apr 85	309	435	326

Table 4 tabulates PP values based on GAB73-74, SPREX-II, GABEX-II, the DOE Report, and from 6 cruises (3 in summer and 3 in winter) along a transect in the inner shelf off of Wassaw Sound [*Verity et al.*, 1993]. The tabulated *in situ* PP estimates are separated by shelf region. Not all data shown in Table 4 were used to derive the regressions of Figure 10. Only the GAB73-74 data were used because they are the only data sets available not affected by the Gulf Stream subsurface summer intrusions. The Wassaw Sound data were extracted from seasonal averages provided in the publication [*Verity et al.*, 1993].

The values in Table 4 indicate a very large seasonal and interannual variability of PP in the inner (38 – 1387), middle (40 – 556), and outer (13 – 360) shelf regions of the SAB. Therefore, the annual estimates vary significantly depending upon which data are used to derive the estimate. Variability in physical forcing, e.g., Gulf Stream intrusions, wind-driven mixing and coastal upwelling, and river discharge, play a major role in the variability. *Haines and Dunstan* [1975] estimated a yearly production of 290 $gC/m^2/yr$ for a broad portion of the SAB inner shelf based on the GAB73-74 data. *Verity et al.* [1993] report a much larger annual PP estimate of 630 – 750 $gC/m^2/yr$ based on the Wassaw Sound transect. However, the lower bound of their estimate may have to be revised to 358 $gC/m^2/yr$ based on the winter and summer estimates for station 6, which appear on page 770 of their paper. *Verity et al.* [1993] attributed the large difference between their estimates and those of *Haines and Dunstan* [1975] to the limited temporal coverage of the latter study, interannual variability, or improvements in methodology (e.g., clean sampling and incubation techniques).

5.5 GABEX-II Summer Intrusion Cruises

Figure 10 implies that seasonal algorithms may be viable. However, summer intrusions were not included. During July and August of 1981 phytoplankton dynamics within Gulf Stream intrusions were investigated in the SAB [*Yoder et al.*, 1985]. The data were collected during the GABEX-II cruises. Resident SAB shelf waters are normally depleted of inorganic nitrogen and

other nutrients. However, plankton productivity is highly affected by upwelling and onshore movement of nutrients driven by eddies and other disturbances of the Gulf Stream front [*Lee and Atkinson*, 1983; *Lee et al.*, 1981]. These upwelling events are the major processes affecting rates

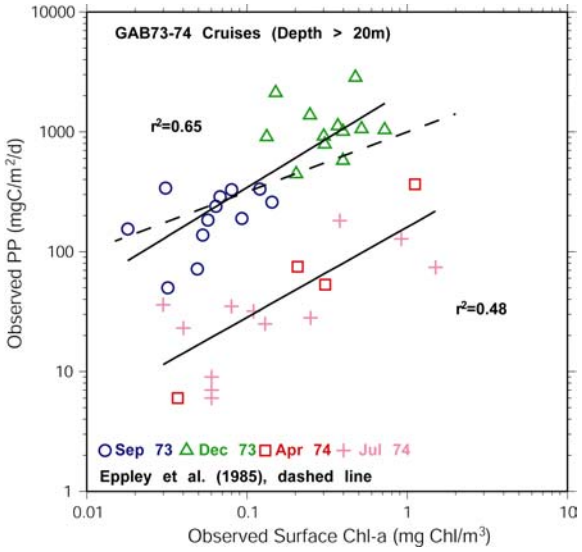

Figure 10. Log-log plot of observed primary production versus observed surface chlorophyll. The two solid lines are fits to the Sep-Dec 73 and Apr-Jul 74 data sets. The dashed line is the *Eppley* et al. (1985) algorithm.

Table 4. Annual PP ($gC/m^2/yr$) based on several SAB data sources. The DOE Report values are also tabulated for comparison. The winter/summer estimates from the Wassaw Sound transect (Station 3 near the coast and Station 6 ~10 km offshore) are reproduced from *Verity et al.* [1993]. The winter means are based on data from 22 January – 12 February 1986, 7 – 29 January 1987, and 5 – 15 January 1988. The summer means are based on data from 13 – 30 August 1985, 11 – 30 July 1986, and 22 June – 17 July 1987.

	Shelf Region		
Data Source	**Inner Shelf**	**Middle Shelf**	**Outer Shelf**
E-13-73 (Sep 73)	268	80	57
E-19-73 (Dec 73)	639	395	360
E-03-74 (Apr 74)	38	48	29
E-12-74 (Jul 74)	69	40	13
GABEX-II (Jul-Aug 81)	---	556	---
SPREX-II (Apr 85)	124	---	---
Summer – Station 3	1387	---	---
Winter – Station 3	113	---	---
Summer – Station 6	621	---	---
Winter – Station 6	95	---	---
DOE (annual mean)	630	248	360

and dynamics of outer shelf and slope (40 to 200m isobaths, Figure 8) primary production [*Atkinson et al.*, 1978; *Bishop et al.*, 1980; *Dunstan and Atkinson*, 1976; *Pomeroy et al.*, 1983; *Yoder*, 1985; *Yoder et al.*, 1983; *Yoder et al.*, 1981a]. Upwelled nutrient-rich Gulf Stream water was a dominant process affecting temporal and spatial changes in phytoplankton biomass and productivity of the SAB continental shelf between 29 and 32°N latitude [*Yoder et al.*, 1985]

during the GABEX-II cruises. The area affected by the intruded waters was very large, including all of the middle and outer shelf and ~50% of the inner shelf area [*Yoder et al.*, 1985]. Integrated *Chl-a* and primary production (PP) within 2 weeks following a large intrusion event on the middle shelf in July reached 3 to 4 gC m^{-2} d^{-1} and 75 mg m^{-2}, respectively [*Yoder et al.*, 1985]. At the peak of the bloom 80% of the water column PP occurred below the mixed layer and new PP (NO_3-supported) exceeded 90% of the total. The intrusion study results imply a seasonal (June to August) middle shelf production of 150 g C m^{-2}, about 15% higher than previous estimates of annual production on the middle shelf. Although intrusions of the scale observed in 1981 may not occur every summer, when they occur they are by far the most important processes controlling summer phytoplankton dynamics of the middle and outer shelf and of the inner shelf in the southern half of the study area [*Yoder et al.*, 1985]. Unfortunately, since most of the production occurs below the mixed layer, it is not possible to use satellite ocean color algorithms to retrieve the effects of these sub-surface blooms on the SAB phytoplankton production.

The location of the GABEX-II stations and the vertical profiles of *Chl-a* and PP are shown in Figure 11. The profiles are separated according to two transects, St. Augustine and Amelia Island transects. Note that both biomass and carbon production increase significantly below 15 meters where Gulf Stream intrusions enhance the nutrient concentration. The subsurface bloom intensity varies from station to station in response to the magnitude of the nutrient enrichment originating from the intrusion. The intrusion effects are more pronounced along the southern (St. Augustine) transect. A plot of the integrated PP versus integrated *Chl-a* originating from both GAB73-74 and GABEX-II data is shown in Figure 12. Two regressions were performed on these data, one combining fall-winter GAB73-74 and summer GABEX-II data (r^2=0.67), and another for the spring-summer GAB73-74 data (r^2=0.32). The dual regressions are consistent with the seasonality of PP previously noted (see Figure 10), e.g., lower production in spring-summer (without intrusions) and higher production in fall-winter, with one difference, the summer intrusion data from GABEX-II overlays the fall-winter GAB73-74 regression. This is consistent with the higher subsurface PP observed during GABEX-II due to Gulf Stream intrusions. Therefore, for years with summer intrusions the PP versus *Chl-a* behavior is identical to fall-winter months. The consequence is that strictly distinct seasonal algorithms suggested by Figure 10 do not hold together when intrusions are present and there is no mechanism for flagging such conditions using the satellite data.

5.6 VGPM2 versus Carbon-Based PP Algorithms

A simple comparison between the VGPM2 and carbon-based algorithms (see Appendix A for description of algorithms) was conducted using input products derived from remote sensing data at the locations of the December 73 and April 74 GAB73-74 stations. SeaWiFS and AVHRR NOAA Coastwatch SAB clear scenes for 13 April and 18 December 2003 were chosen for the comparison. The SeaWiFS-derived products are PAR, GSM01 *Chl-a*, GSM01 backscatter coefficient at 443 nm (b_{bp}), and diffuse attenuation coefficient at 490 nm (K_{490}). SST was derived from NOAA Coast Watch AVHRR scenes for the same days. Concurrent daily mixed layer depth data were obtained from the Fleet Numerical Meteorology and Oceanography Center (FNMOC). Figure 13 shows the scatter plot of VGPM versus carbon-based algorithms. The carbon-based algorithm shows a consistent positive bias when compared to the VGPM (RPD=64% and APD=70%).

5.7 Summary

- The observed SAB PP reveals strong seasonal and interannual variability.

- The VGPM2 algorithm did not provide consistent accurate retrievals of PP when forced with SST, *Chl-a*, and PAR from *in situ* data. Specifically, the large seasonal variability is not captured by the algorithm because PP and chlorophyll concentration are seasonally decoupled.

- The significant interannual variability on the inner shelf during April is probably due to changes in river discharge (turbidity), which imparts on light limitation on PP.

- An empirical seasonally dependent algorithm is offered based on regression between PP and surface chlorophyll.

- A comparison between the VGPM2 and carbon-based algorithms was performed for the same months (April and December) and at the locations of E-19-73 and E-03-74 stations using inputs from SeaWiFS (*Chl-a*, backscatter coefficient, and PAR) and AVHRR (SST) satellite sensors, and daily FNMOC mixed layer depth. The carbon-based algorithm shows a consistent positive bias when compared with to the VGPM2 (RPD=64%, APD=70%).

- Data from the GABEX-II summer intrusion study were analyzed. These data show significant subsurface (below mixed layer) blooms that occur during episodical Gulf Stream intrusions. Therefore, it is not possible to use satellite ocean color algorithms to retrieve the effects of these sub-surface blooms on the SAB phytoplankton production.

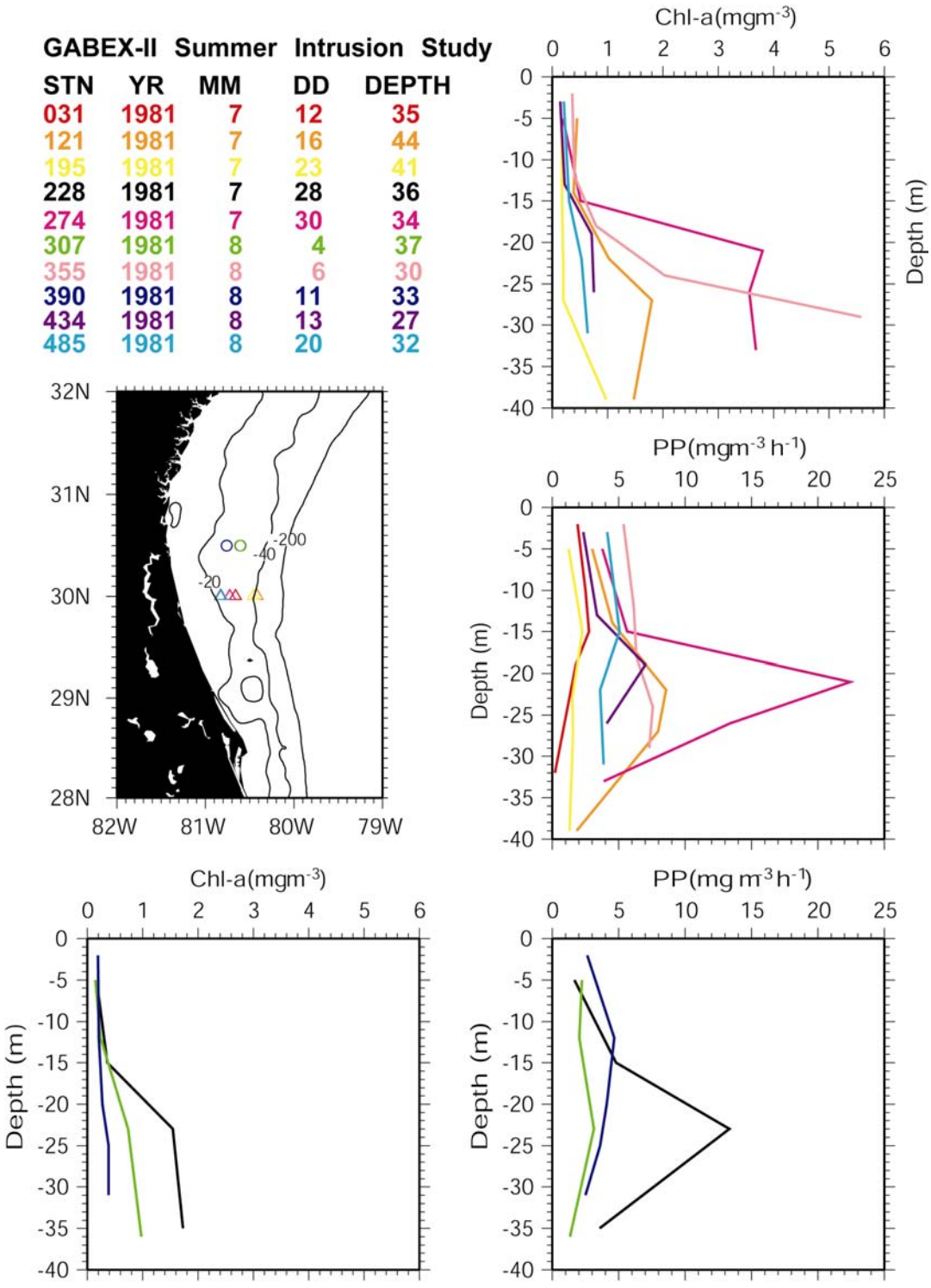

Figure 11. Vertical profiles of *Chl-a* and PP from the 1981 summer intrusion study (GABEX-II). A map of station locations, and a tabulation of date and depth for each station, is shown in the upper left side of the figure. The station locations and corresponding profiles are color coded according to the tabulation. The triangles correspond to the St. Augustine transect (top and middle profiles on the right), while the circles correspond to the Amelia Island transect (left and right bottom profiles).

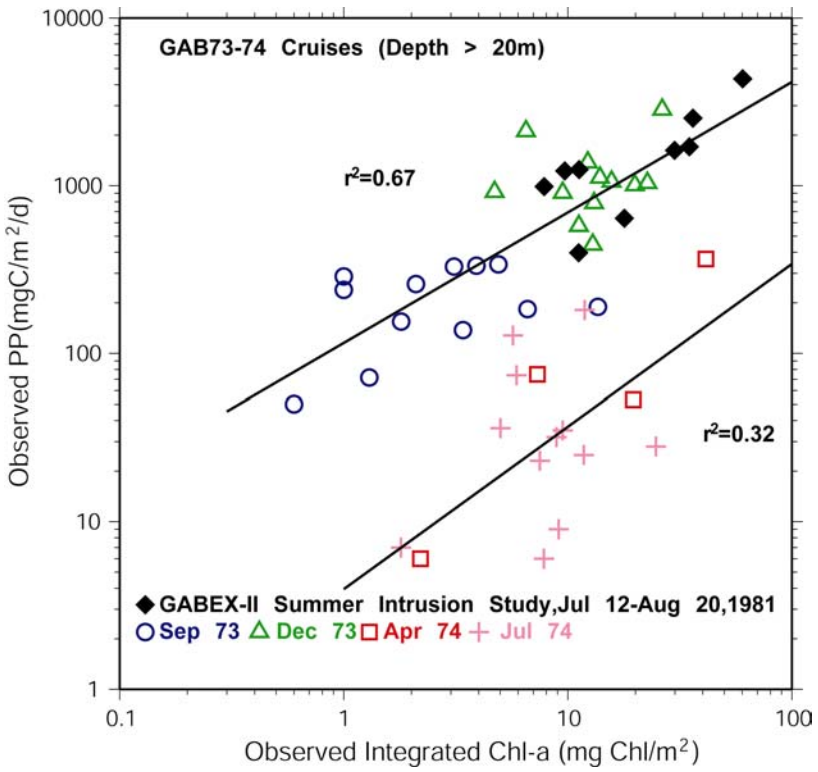

Figure 12. Observed integrated PP versus observed integrated *Chl-a* from GAB73-74 and GABEX-II cruises. Two regression lines are shown, one for a combination of GAB73-74 (September and December 73) and GABEX-II (July and August 1981) data (r^2=0.67), and another for the spring-summer (April and July 74) GAB73-74 data (r^2=0.32).

6. Chesapeake Bay CDOM and DOC Analysis

In situ observations of chromophoric dissolved organic matter (CDOM) absorption coefficient (a_{CDOM}) and dissolved organic carbon (DOC) are being made at four stations across the mouth of Chesapeake Bay [*A. Mannino*'s personal communication]. An initial attempt was made to develop a remote sensing algorithm to retrieve DOC with the limited data available to date. The algorithm strategy and equations are given in Appendix A. Data from five cruises, 5 July, 1 September, 15 October, and 15 November 2004, and 10 January 2005 were available for this study. However, only the July, September, and October 2004 data had concurrent SeaWiFS retrievals available for analysis. Table 5 summarizes the results.

Two algorithms are required to obtain the DOC retrievals from space. First, we used the algorithms of *Johannessen et al.* [2003] to get the diffuse attenuation, K_d, and a_{CDOM} at 380 nm. This is a two-step process since a_{CDOM} is a function of K_d in this method. Second, we used seasonally dependent regressions of DOC versus $a_{CDOM}(380)$ to obtain the DOC retrievals [*A. Mannino*, unpublished manuscript]. Note in Table 5 that the DOC retrievals are much more accurate (RPD of 3 – 40%) when the a_{CDOM} retrievals are also more accurate (RPD of 0 – 47%). This means that an improvement on the a_{CDOM} algorithm will have a large impact on the

Table 5. Observed versus SeaWiFS-derived CDOM absorption coefficient (a_{CDOM}, in m^{-1}) at 380 nm and DOC (μM C).

		$a_{CDOM}(380)$			DOC		
Date	**Stn**	**In Situ**	**SeaWiFS**	**RPD(%)**	**In Situ**	**SeaWiFS**	**RPD(%)**
7/05/04	3A	0.78	1.16	49	183	310	69
9/01/04	3A	1.06	0.79	-26	199	174	13
10/15/04	3A	0.74	1.69	128	141	430	205
7/05/04	7	0.81	1.10	36	217	293	35
9/01/04	7	0.87	0.77	-12	196	173	-12
10/15/04	7	0.94	1.92	104	170	499	194
7/05/04	11	0.62	0.91	47	177	242	37
9/01/04	11	0.67	0.64	-5	162	155	-4
10/15/04	11	0.78	1.94	149	159	505	218
7/05/04	17	0.60	0.96	60	160	254	59
9/01/04	17	0.60	0.60	0	146	150	3
10/15/04	17	0.90	1.80	100	196	462	136

accuracy of the DOC retrievals. Also note that the worst retrievals occurred in October and the best occurred in July and September. This is consistent with the data used to develop the regressions for K_d and a_{CDOM}, which consisted of a total of 6 stations in Chesapeake and Delaware Bays in the summers of 1996, 1997, and 1998. Therefore there is a seasonal bias in the algorithm and the number of data points is not sufficient for the development of a robust algorithm. However, these preliminary results are very encouraging and the current acquisition of additional data will contribute to the development of more accurate algorithms.

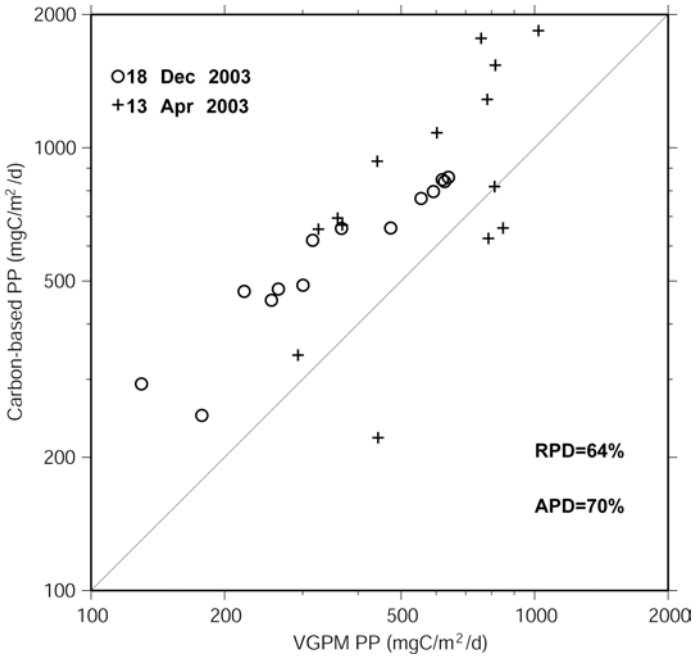

Figure 13. Scatter plot of VGPM versus carbon-based PP algorithms using satellite-derived input parameters. The relative (RPD) and absolute percent differences (APD) are shown inside the figure.

Appendix A
Algorithm Description

A.1 Chlorophyll Algorithms

Three different types of *Chl-a* algorithms were evaluated for the South Atlantic Bight (SAB) and Chesapeake Bay (CB), empirical, semi-analytical, and hybrid (empirical and semi-analytical). The two empirical, or band ratio, algorithms are the OC4v4 [*O'Reilly et al.*, 2000] and the Clark (unpublished) algorithms. The semi-analytical algorithm is the Garver-Siegel-Maritorena (GSM01) algorithm [*Maritorena et al.*, 2002], and the hybrid algorithm is the Carder algorithm [*Carder et al.*, 2004a; *Carder et al.*, 1999]. The following is a description of each of these chlorophyll algorithms.

A.1.1 OC4v4 Empirical Algorithm

$$\begin{aligned} &\mathrm{Chl}=10^{(0.366-3.067R_{4S}+1.930R_{4S}^2+0.649R_{4S}^3-1.532R_{4S}^4)} \\ &\text{where, } R_{4S}=\log_{10}\left(R_{555}^{443}>R_{555}^{490}>R_{555}^{510}\right) \end{aligned} \tag{A.1}$$

and the argument of the logarithm is a shorthand representation for the maximum value of the three reflectance ratios.

A.1.2 Clark's Empirical Algorithm

$$\begin{aligned} &\mathrm{Chl}=10^{\left(0.819199-3.297494x+7.682118x^2-17.612831x^3+18.69251x^4-7.302652x^5\right)} \\ &\text{where,}\quad x=\log_{10}\left(\frac{nLw(443)+nLw(490)}{nLw(555)}\right) \end{aligned} \tag{A.2}$$

and $nLw(443)$, $nLw(490)$, and $nLw(555)$ are the normalized water-leaving radiances at each respective wavelength.

A.1.3 GSM01 Semi-Analytical Algorithm

The semi-analytical algorithm is the GSM01 [*Garver and Siegel*, 1997; *Maritorena et al.*, 2002], which relates refletances (*Rrs*), Chl, and inherent optical properties (IOPs) via the equation:

$$Rrs(\lambda)=\frac{t}{n_w^2}\sum_{i=1}^{2}g_i\left\{\frac{b_{bw}(\lambda)+b_{bp}(\lambda_o)(\lambda/\lambda_o)^{-\eta}}{b_{bw}(\lambda)+b_{bp}(\lambda_o)(\lambda/\lambda_o)^{-\eta}+a_w(\lambda)+\mathrm{Chl}\,a_{ph}^*(\lambda)+a_{dg}(\lambda_o)\exp\left[-S(\lambda-\lambda_o)\right]}\right\}^i \tag{A.3}$$

where t is the sea-air transmission factor and n_w is the index of refraction of the water. The IOP spectra, $a(\lambda)$ and $b_b(\lambda)$, are partitioned into relevant components of seawater backscatter $b_{bw}(\lambda)$ and absorption $a_w(\lambda)$, particulate backscatter $b_{bp}(\lambda)$, phytoplankton absorption $a_{\mathrm{ph}}(\lambda)$, and the combined dissolved and detrital particulate absorption coefficients $a_{\mathrm{dg}}(\lambda)$. Values of $a_w(\lambda)$ and $b_{bw}(\lambda)$ are assumed to be known constants [*Morel*, 1974; *Pope and Fry*, 1997]. The IOP spectra for phytoplankton, combined dissolved and detrital particulate absorption, and particulate backscatter are parameterized in terms of known shape with an unknown magnitude taken from the literature:

$$a_{ph}(\lambda) = \mathrm{Chl}\ a_{ph}^{*}(\lambda), \tag{A.4a}$$

$$a_{dg}(\lambda) = a_{dg}(\lambda_o)\ \exp[-S(\lambda-\lambda_o)], \tag{A.4b}$$

$$b_{bp}(\lambda) = b_{bp}(\lambda_o)\ (\lambda/\lambda_o)^{-\eta}, \tag{A.4c}$$

where $a_{ph}^{*}(\lambda)$ is the *Chl-a* specific absorption coefficient, S is the spectral decay constant for cdm absorption [*Bricaud et al.*, 1981; *Green and Blough*, 1994], η is the power-law exponent for the particulate backscattering coefficient, and λ_o is a scaling wavelength (443 nm). The unknown magnitudes in equations 4a, 4b, and 4c are *Chl-a*, $a_{dg}(\lambda_o)$, and $b_{bp}(\lambda_o)$, respectively. Equation (3) is the complete functional form of the inversion model. The g_i terms (0.0949, 0.0794) are fitting coefficients from Monte Carlo simulations of an idealized ocean [*Gordon*, 1986]. With a set of globally optimized values for η, S, and $a_{ph}^{*}(\lambda)$ [*Maritorena et al.*, 2002], and applying a non-linear least squares fit function (Levenberg-Marquard) to equation (3), the three unknowns, *Chl-a*, $a_{dg}(443)$, and $b_{bp}(443)$ can be determined. Table A-1 shows the optimized input parameters.

Table A-1. Parameter values for globally optimized GSM01 semi-analytical algorithm.

Parameter	Value
$a_{ph}^{*}(412)$	0.00665
$a_{ph}^{*}(443)$	0.05582
$a_{ph}^{*}(490)$	0.02055
$a_{ph}^{*}(510)$	0.01910
$a_{ph}^{*}(555)$	0.01015
$a_{ph}^{*}(670)$	0.01424
S	0.02061
η	1.0337

The GSM01 algorithm was optimized for Chesapeake Bay waters by *Maguson et al.* [2004]. The optimized parameters for this regionally tuned algorithm (GSM01-CB) are given in Table A-2.

A.1.4 Carder's Semi-Analytical/Empirical Algorithm

The algorithm switches from semi-analytical to empirical (default) modes according to the value of the phytoplankton absorption coefficient at 675 nm, $a_{ph}(675)$. For waters with high concentrations of CDOM and chlorophyll, $nL_w(412)$ and $nL_w(443)$ values are small and the semi-analytical algorithm cannot perform properly. Therefore, the algorithm is designed to retrieve

Table A-2. Optimized parameters for GSM01-CB, regionally and seasonally divided [*Magnuson et al.*, 2004]. The regional domains are defined as upper Bay (north of 38.6°N), mid-Bay (37.6 – 38.6°N), and lower Bay (south of 37.6°N). The inshore-offshore regions (*) of the Middle Atlantic Bight (MAB) are divided by a line running parallel to the shoreline a distance of ~30-40 km from the coast.

Region	Season	a_{ph}*(412)	a_{ph}*(443)	a_{ph}*(490)	a_{ph}*(510)	a_{ph}*(555)	a_{ph}*(670)	S_{dg}	η
Upper Bay	**Spring**	0.02119	0.02509	0.01282	0.00910	0.00427	0.02087	0.01218	0
	Summer	0.02653	0.02979	0.01655	0.01208	0.00470	0.02122	0.01218	0
	Fall	0.02259	0.02573	0.01372	0.01019	0.00376	0.02066	0.01218	0
Mid-Bay	**Spring**	0.02001	0.02212	0.01279	0.00974	0.00449	0.01588	0.01385	0
	Summer	0.03345	0.03900	0.02318	0.01664	0.00609	0.02285	0.01385	0
	Fall	0.02758	0.03080	0.01826	0.01438	0.00691	0.02112	0.01385	0
Lower Bay	**Spring**	0.02001	0.02212	0.01279	0.00974	0.00449	0.01588	0.01330	0
	Summer	0.03345	0.03900	0.02318	0.01664	0.00609	0.02285	0.01330	0
	Fall	0.02758	0.03080	0.01826	0.01438	0.00691	0.02112	0.01330	0
Inshore		0.07123	0.08843	0.06024	0.04072	0.01693	0.03815	0.01236	0
Offshore		0.11331	0.14678	0.09832	0.06048	0.01920	0.04349	0.01646	1

* The longitude of the inshore-offshore boundary is defined for latitude south of 37°N as longitude = (latitude-153.31)/1.5385, and for latitude north of 37°N as longitude = -(latitude+152)/2.5. The line orientation changes from SE-NW south of 37°N, to SW-NE north of 37°N.

values only when modeled $a_{ph}(675)$ is less than 0.03 m^{-1}, which is equivalent to *Chl-a* concentrations of ~1.5-2.0 mg m^{-3}. The empirical mode is invoked for $a_{ph}(675) \geq 0.03$ m^{-1}. In addition, by comparing the sea-surface temperature to the nitrate depletion temperature (NDT) [*Kamykowski*, 1987], the presence of large, chlorophyll-rich cells and small, chlorophyll-poor cells can be deduced from space [*Carder et al.*, 1999]. Chlorophyll-rich cells with low $a_{ph}^*(\lambda)$ values (packaged pigments) are generally present in photon-poor, nutrient replete environments, whereas chlorophyll-poor cells with high $a_{ph}^*(\lambda)$ values (unpackaged pigments) are present in photon-rich, nutrient-deplete environments. The NDT for any region of the ocean is the temperature above which nitrate is negligible. Weighting functions are used to make the transitions between semi-analytical to empirical modes, and from packaged to unpackaged situations more smoothly. The following is a description of the algorithm equations and parameters used with the algorithm for SeaWiFS wavebands.

Semi-Analytical Component

The reflectance model, which is adapted from *Lee et al.* [1994], is given by:

$$R_{rs} = \frac{f\,t^2}{Q(\lambda)\,n^2}\,\frac{b_b(\lambda)}{\left[a(\lambda)+b_b(\lambda)\right]} \tag{A.5}$$

where f is an empirical factor averaging 0.32-0.33 [*Gordon et al.*, 1975; *Jerome et al.*, 1988; *Kirk*, 1991; *Morel and Prieur*, 1977], t is the transmittance of the air-sea interface, $Q(\lambda)$ is the upwelling irradiance-to-radiance ratio $E_u(\lambda)/L_u(\lambda)$, n is the real part of the index of refraction of seawater. Equation A.5 can be greatly simplified by performing the following approximations: (1) t^2/n^2 is ~0.54, and, although it may change with sea state [*Austin*, 1974], it is relatively independent of wavelength, and (2) except for highly turbid waters, $b_b(\lambda)$ is usually much smaller than $a(\lambda)$ and therefore can be removed from the denominator of A.5. Thus, for the SeaWiFS 412, 443, and 555 nm bands we can use A.6 to derive the following equations:

$$\frac{R_{rs}(412)}{R_{rs}(443)} = \frac{b_b(412)\,a(443)}{b_b(443)\,a(412)} \tag{A.6}$$

$$\frac{R_{rs}(443)}{R_{rs}(555)} = \frac{b_b(443)\,a(555)}{b_b(555)\,a(443)} \tag{A.7}$$

As it will be shown later, the right hand side of each of the above equations is a function of $a_{ph}(675)$, $a_{dg}(400)$, $R_{rs}(443)$, $R_{rs}(490)$, and $R_{rs}(555)$. The R_{rs} values are known from the satellite data. Thus we have a set of two equations and two unknowns, which can be numerically solved.

The backscatter coefficient can be expanded into its water and particle components as,

$$b_b(\lambda) = b_{bw}(\lambda) + b_{bp}(\lambda) \tag{A.8}$$

The backscatter coefficient for water is well known [*Baker and Smith*, 1982]; $b_{bp}(\lambda)$ is modeled as

$$\begin{aligned} b_{bp}(\lambda) &= X\left[\frac{555}{\lambda}\right]^{Y} \\ X &= X_o + X_1 R_{rs}(555) \\ Y &= Y_o + Y_1 \frac{R_{rs}(443)}{R_{rs}(490)} \end{aligned} \tag{A.9}$$

where X_o, X_1, Y_o, Y_1 are constants (see Table A-3).

The total absorption term, $a(\lambda)$, can be expanded into its water, phytoplankton, and detritus plus

gelbstoff (CDOM) components. The water absorption coefficient is known [*Pope and Fry*, 1997]. The remaining components of the absorption coefficient are developed as follows. The phytoplankton absorption coefficient is written as function of $a_{ph}(675)$,

$$a_{ph}(\lambda) = a_0(\lambda)\exp\left[a_1(\lambda)\tanh\left[a_2(\lambda)\ln\left(a_{ph}(675)/a_3(\lambda)\right)\right]\right]a_{ph}(675) \quad \text{(A.10)}$$

where a_0, a_1, a_2, and a_3 are wavelength dependent parameters (see Table A-4).

The combined CDOM and detritus absorption coefficient is written as,

$$a_{dg}(\lambda) = a_{dg}(400)\exp\left[-S(\lambda - 400)\right] \quad \text{(A.11)}$$

Table A-3. Wavelength-independent parameters for the semi-analytical chlorophyll algorithm for regions without package pigments (unpackaged), packaged, highly packaged, and globally packaged. Note that several parameters do not change with the level of packaging.

Param	Unpkg	Packaged	Hipkg	Global
X_0	-0.00182	-0.00182	-0.00182	-0.00182
X_1	2.058	2.058	2.058	2.058
Y_0	-1.13	-1.13	-1.13	-1.13
Y_1	2.57	2.57	2.57	2.57
S	0.0225	0.0225	0.0225	0.0225
P_0	1.7150	1.7739	1.9000	1.7454
P_1	1.00	1.00	1.00	1.00
c_0	0.2818	0.423284	0.51	0.354824
c_1	-2.783	-2.50834	-2.340	-2.64124
c_2	1.863	0.45994	0.40	1.13884
c_3	-2.387	-0.90706	0.0	-1.62316

The semi-analytical model can now be inverted on a pixel-by-pixel basis for each of the six (412, 443, 490, 510, 555, and 670 nm) SeaWiFS bands (or MODIS visible bands 412, 443, 488, 510, and 551) for two unknowns ($a_{ph}(675)$ and $a_{dg}(400)$) using equations A.6 through A.11.

The *Chl-a* algorithm for the semi-analytical case, when an acceptable value of $a_{ph}(675)$ is returned (<0.03 m^{-1}), is calculated from,

$$Chl\text{-}a = P_0\left[a_{ph}(675)\right]^{P_1} \quad \text{(A.12)}$$

Empirical (Default) Algorithm

Empirical algorithms are used when the semi-analytical algorithm does not return a valid value for $a_{ph}(675)$, usually due to low values of $R_{rs}(412)$ in eutrophic waters. The empirical algorithms for chlorophyll, absorption and backscatter coefficients [*Carder et al.*, 2004b] are :

$$a_{ph}(675)_{\text{emp}} = 0.328 \times 10^{\left(-0.919+1.037 r_{25}-0.407 r_{25}^2-3.531 r_{35}+1.702 r_{35}^2-0.008\right)} \tag{A.13}$$

$$a_{dg}(400)_{\text{emp}} = 1.5 \times 10^{\left(-1.147-1.963 r_{15}-1.01 r_{15}^2+0.856 r_{25}+1.702 r_{25}^2\right)} \tag{A.14}$$

$$\left[\text{chl-a}\right]_{\text{emp}} = 10^{\left(0.354824-2.64124 \log(r_{35})+1.13884\left[\log(r_{35})\right]^2-1.62316\left[\log(r_{35})\right]^3\right)} \tag{A.15}$$

$$r_{15} = \frac{R_{rs}(412)}{R_{rs}(555)} \quad r_{25} = \frac{R_{rs}(443)}{R_{rs}(555)} \quad r_{35} = \frac{R_{rs}(490)}{R_{rs}(555)}$$

Weighted Chlorophyll Algorithm

An important consideration is that there should be a smooth transition in *Chl-a* values when the algorithm switches from the semi-analytical (*sa*) to the empirical (*emp*) method. When the semi-analytical algorithm returns an $a_{ph}(675)$ value between 0.015 and 0.03 m^{-1}, *Chl-a* is calculated as

$$Chl\text{-}a = w_1\left[Chl\text{-}a\right]_{sa} + (1-w_1)\left[Chl\text{-}a\right]_{emp} \tag{A.16}$$

where the weighting factor is w_1=[0.03-$a_{ph}(675)$]/0.015. The transition between the different levels of pigment packaging is controlled by a weighting function that is proportional to SST and NDT:

$$Chl\text{-}a = w_2\left[Chl\text{-}a\right]_{\text{TP1}} + (1-w_2)\left[Chl\text{-}a\right]_{\text{TP2}} \tag{A.17}$$

where the weighting function w_2 and the type of packaging coefficients to be used (TP1 and TP2) in the calculation of the interpolated *Chl-a* value for each SST range are given in Table A-5.

A.2 Primary Production Algorithms

Three ocean color primary production (PP) algorithms were analyzed with inputs from both satellite and *in situ* data. The chlorophyll-based vertically generalized production model

(VGPM), originally developed by *Behrenfeld and Falkowski* [1997], the recently published carbon-based production model [*Behrenfeld et al.*, 2005], and the chlorophyll-based PP algorithm regionally developed for the Southern California Bight [*Eppley et al.*, 1985]. A modified version of the VGPM, hereafter VGPM2, was used instead. Specifically, this modified version replaces the polynomial function of SST for the optimal assimilation efficiency of the productivity profile (P^B_{opt}) with the product of the maximum achievable specific growth rate, an exponential function of temperature [*Eppley*, 1972], and a constant carbon to chlorophyll ratio. The following subsections describe these PP algorithms.

VGPM2

The *PP*, in mg C m^{-2} d^{-1}, is written as,

$$PP = Chl_{sat} \times Z_{eu} \times P^{B}_{opt} \times DL \times F(E_0) \quad \text{(A.18)}$$

Table A-4. Wavelength-dependent parameters for the semi-analytical chlorophyll algorithm for regions without packaged pigments (unpkg), packaged (pkg), highly packaged (hipkg), globally packaged (global). Note that several coefficients do not change with the level of pigment packaging or wavelength.

	Wavelength					
Parameter	**412**	**443**	**490**	**510**	**555**	**670**
b_{bw}(m^{-1})	0.003341	0.002406	0.001563	0.001313	0.000929	0.000388
a_w(m^{-1})	0.004641	0.007098	0.015267	0.032599	0.059649	0.440188
a_0(unpkg)	2.20	3.59	2.27	1.40	0.42	1.00
a_1(unpkg)	0.59	0.69	0.54	0.35	-0.18	0.00
a_2(unpkg)	-0.48	-0.48	-0.48	-0.48	-0.48	-0.48
a_3(unpkg)	0.0112	0.0112	0.0112	0.0112	0.0112	0.0112
a_0(pkg)	1.46778	2.53786	1.62954	1.04970	0.355520	1.00
a_1(pkg)	0.59	0.69	0.54	0.35	-0.18	0.00
a_2(pkg)	-0.48	-0.48	-0.48	-0.48	-0.48	-0.48
a_3(pkg)	0.017276	0.017276	0.017276	0.017276	0.017276	0.017276
a_0(hipkg)	1.019	1.893	1.237	0.835	0.316	1.00
a_1(hipkg)	0.26	0.45	0.42	0.36	-0.08	0.00
a_2(hipkg)	-0.45	-0.45	-0.45	-0.45	-0.45	-0.45
a_3(hipkg)	0.021	0.021	0.021	0.021	0.021	0.021
a_0(global)	1.82	3.05	1.94	1.22	0.39	1.00
a_1(global)	0.59	0.69	0.54	0.35	-0.18	0.00
a_2(global)	-0.48	-0.48	-0.48	-0.48	-0.48	-0.48
a_3(global)	0.014	0.014	0.014	0.014	0.014	0.014

where Chl_{sat} is the satellite surface chlorophyll (mg m^{-3}), Z_{eu} is the euphotic depth (m, 1% of surface photosynthetic available radiation, PAR) calculated using Chl_{sat} and *Morel and Berthon* [1989], *DL* is the day length (h), and P^B_{opt} and the light function $F(E_0$=surface PAR in moles-quanta m^{-2} d^{-1}) are given by

$$P_{\text{opt}}^{\text{P}} = 1.54 \times 10^{(0.0275 \times \text{SST} - 0.07)} \tag{A.19}$$

Table A-5. Tabulation of weighting function and type of packaging coefficients, as a function of SST, to be used in the interpolation of *Chl-a* retrievals in transitional zones (see equation 18).

SST Range	w_2	TP1	TP2
SST ≥ NDT+3.0	1.0	unpkg	---
NDT+0.8 ≤ SST < NDT+3.0	(SST-(NDT+3.0))/3.8	unpkg	global
NDT-0.1 ≤ SST < NDT+0.8	(SST-(NDT-0.1))/0.9	pkg	global
NDT-2 ≤ SST < NDT-0.1	(SST-(NDT-2))/1.9	pkg	hipkg
SST < NDT-2	1.0	hipkg	---

$$F(E_0) = 0.66125 \frac{E_0}{E_0 + 4.1} \tag{A.20}$$

Carbon-Based PP Model

The carbon-based model *PP*, in mg C m^{-2} d^{-1}, is written as,

$$PP = C_{\text{sat}} \times \mu \times F(E_0) \times Z_{\text{eu}} \tag{A.21}$$

where the satellite phytoplankton carbon C_{sat} (mg C m^{-3}), the phytoplankton growth rate μ (d^{-1}), and the euphotic depth Z_{eu} (m) are given by

$$C_{\text{sat}} = 13000\left(b_{bp} - 0.00035\right) \tag{A.22}$$

$$\mu = \mu_{\max} \, Chl:C / (Chl:C)_{\max} \left[1 - \exp\left(-3.0 I_g\right)\right] \tag{A.23}$$

$$\left(Chl:C\right)_{\max} = 0.022 + \left(0.044 - 0.022\right)\exp\left(-3.0 I_g\right) \tag{A.24}$$

$$I_g = I_o \exp\left(-K_{490}\text{MLD}/2\right)/dayL \tag{A.25}$$

$$Z_{eu} = -\ln(0.01)/K_{490} \tag{A.26}$$

where μ=2.0 d^{-1}, I_g (mole-quanta m^{-2}) is the median mixed layer light level, I_o (mole-quanta m^{-2} h^{-1}) is the surface PAR, K_{490} is the diffuse attenuation coefficient at 490 nm, and *dayL* is the day length in hours.

A.3 POC Algorithms

A total of six POC algorithms are presented here: the Clark algorithm (*Clark, unpublished manuscript*) and five other algorithms [*Stramska and Stramski*, 2005], hereafter referred to as Stramski algorithms. The units are in mg C/L for the Stramski algorithms and μg C/L for the Clark algorithm. The algorithm equations are shown below.

A.3.1 The Clark Algorithm

The *in situ* optical and POC data used to develop the Clark algorithms originates from open-ocean and coastal regions, including Chesapeake Bay, where POC concentrations are much higher. However, the actual range of *in situ* POC values used in the algorithm development is not available. The algorithm equations are:

$$\mathrm{POC}=10^{y}\text{, in mg C/liter} \tag{A.27}$$

where,

$$y = a\,(\log x)^5 + b\,(\log x)^4 + c\,(\log x)^3 + d\,(\log x)^2 + e\,(\log x) + f$$

$$x = (nLw(443)+nLw(490))/nLw(555)$$

a = -7.364709, b=19.96593, c=-19.569603, d=8.745837,

e = -3.228108, f=-0.161387

A.3.2 Stramski Algorithms

The data to develop these algorithms, *in situ* reflectances and POC concentration, originate from several programs. These are: CalCOFI (1998), BATS (1998), HOT (1998), JGOFS Arabian Sea (1995), and JGOFS Southern Ocean (1997-1998). The POC concentrations from these data sets range from 20 to 1000 mg m^{-3}. POC from these algorithms is measured in mg C m^{-3}.

Stramski-1: based on beam attenuation coefficient of particles at 660 nm

$$c_p(660) = 1.0976 \exp(-0.7542\,Lr) \tag{A.28}$$

$$Lr = nLw(443)/nLw(555) \tag{A.29}$$

$$\mathrm{POC} = 557.30\,c_p(660)^{1.3121} \tag{A.30}$$

Stramski-2: based on backscatter coefficient at 589 nm

$$b_b(589) = 0.0069\,nLw(555) - 0.0005 \tag{A.31}$$

$$\mathrm{POC} = 179557\,b_b(589) - 137.68 \tag{A.32}$$

Stramski-3: based on chlorophyll concentration

$$\mathrm{POC} = 35.827\ \mathit{Chl\text{-}a} + 22.177 \tag{A.33}$$

Stramski-4: based on blue/green reflectance ratios

$$\mathrm{POC} = 232.1454\ x^{-1.4651} \tag{A.34}$$

$$x = \mathit{Rrs}(490)/\mathit{Rrs}(555) \tag{A.35}$$

Stramski-5: based on blue/green reflectance ratios

$$\mathrm{POC} = 196.1637\ x^{-1.1141} \tag{A.36}$$

$$x = \mathit{Rrs}(443)/\mathit{Rrs}(555) \tag{A.37}$$

The first three algorithms (Stramski-1, -2, -3) were developed using data from the North Polar Atlantic, while the last two algorithms (Stramski-4, -5) were derived with data from the Arabian Sea, Bermuda Atlantic Time Series (BATS) and Hawaii Ocean Time (HOT) series sites. Therefore, only the Stamski-4 and –5 algorithms were tested, as they are based on a broader variety of bio-optical environments and thus more appropriate for use in Middle Atlantic Bight (MAB) waters. The Stramski algorithm is based on open ocean observations and may not be valid for coastal and estuarine waters where POC values can be much higher.

A.4 CDOM and DOC Algorithms

The DOC retrievals were obtained using a two-stage process. First, K_d and a_{CDOM} at 380 nm were retrieved using the regressions of *Johannessen et al*. [2003] for Delaware and Chesapeake Bays. Second, seasonally dependent regressions of DOC versus $a_{\mathrm{CDOM}}(380)$ [*A. Mannino*, personal communication] were used to retrieve the DOC concentrations. The regression equations and coefficients are given below.

$$K_d(380) = 0.302\left[\mathit{Rrs}(412)/\mathit{Rrs}(555)\right]^{-1.24} \tag{A.38}$$

$$a_{\mathrm{CDOM}}(380) = 0.183K_d(380) + 0.40 \tag{A.39}$$

$$\mathrm{DOC} = \left[a_{\mathrm{CDOM}}(380) - a\right]/b \tag{A.40}$$

The *a* and *b* seasonal coefficients are given in Table A-6.

Table A-6. Regression and correlation coefficients for the DOC versus a_{CDOM} equation.

Date	***a***	***b***	$\mathbf{r^2}$
7/05/04	0.02359	0.00368	0.68
9/01/04	-0.53084	0.00756	0.89
10/15/04	0.30053	0.00324	0.59
11/15/04	-0.23285	0.00661	0.98
1/10/05	-0.51667	0.00815	0.99

Appendix B
Description of Match-up Process

A step-by-step description of the match-up procedure is provided in this appendix. A flow chart of the entire procedure (sequenced 1 through 15) is provided in Figure B.1. Each in situ record undergoes the following process on the way to becoming a valid match-up record:

1) A query is made to the Ocean Color Data Processing System (ODPS) to find coincident satellite data. This query requires: date, time, latitude, longitude, and satellite sensor.

2) If a coincident satellite Level 1 (L1) file is located, the file is extracted to produce a (nominally) 101x101 pixel subset. The location (pixel/line) within the extract that most closely matches the latitude/longitude of the in situ data is recorded.

3) The extracted L1 file is processed to L2, outputting all products of interest, as well as some appropriate ancillary information (e.g. zenith angles, l2flags, aerosol models, etc.)

During the extraction process, the following occurs:

- Masks applied are: LAND, HIGLINT, HILT, STRAYLIGHT, CLDICE, ATMFAIL, LOWLW, FILTER, and valid pixel count is calculated based on the above masks.
- Non-flagged pixels are averaged
- Standard deviation of the non-flagged (unmasked) pixels is calculated
- Filtered mean (values within ±1.5 standard deviations of the median) is calculated
- New valid pixel count determined from filtered mean
- A total pixel count determined (box size (5x5 pixels) minus land pixels)
- Calculation of mean, median, standard deviation (stdev), filtered mean, filtered mean stdev, min/max values and filtered pixel count, for each product as well as valid pixel count, and non-land pixel count for the 5x5 box

After the extraction process is completed, the following statistical information is calculated and stored in a relational database. The coefficient of variation (CV) is determined for the satellite record. This is calculated as the median of the combined ratios of stdev/mean for the normalized water-leaving radiances, $nLw(\lambda)$, in the visible bands between 405 and 570nm, as well as $\tau(865)$, the aerosol optical thickness, for all the valid pixels. The satellite record filtered pixel count is determined as the minimum of the filtered pixel count for all products. After the above statistical information is obtained, the exclusion criteria begins following the criteria below:

- Time window: ±10800 sec (3 hrs)
- Minimum number of pixels unmasked: 50%
- CV Failure: > 0.15
- Eliminate duplicate source data (GAC, HRPT, MLAC) useful only for SeaWiFS
- Geometry extremes: Maximum solar zenith (Solz) allowed is 75^{o}; maximum sensor zenith (Senz) allowed is 60^{o}
- Failed downwelling irradiance, *Es,* threshold: 80% > (in situ *Es*/theoretical clear sky *Es*) > 120%
- If there are multiple orbits choose the closest in time
- Exceeded distance criteria: multiple in situ measurements must be far enough apart so as to be a unique (up to 5x5 pixels) satellite averages

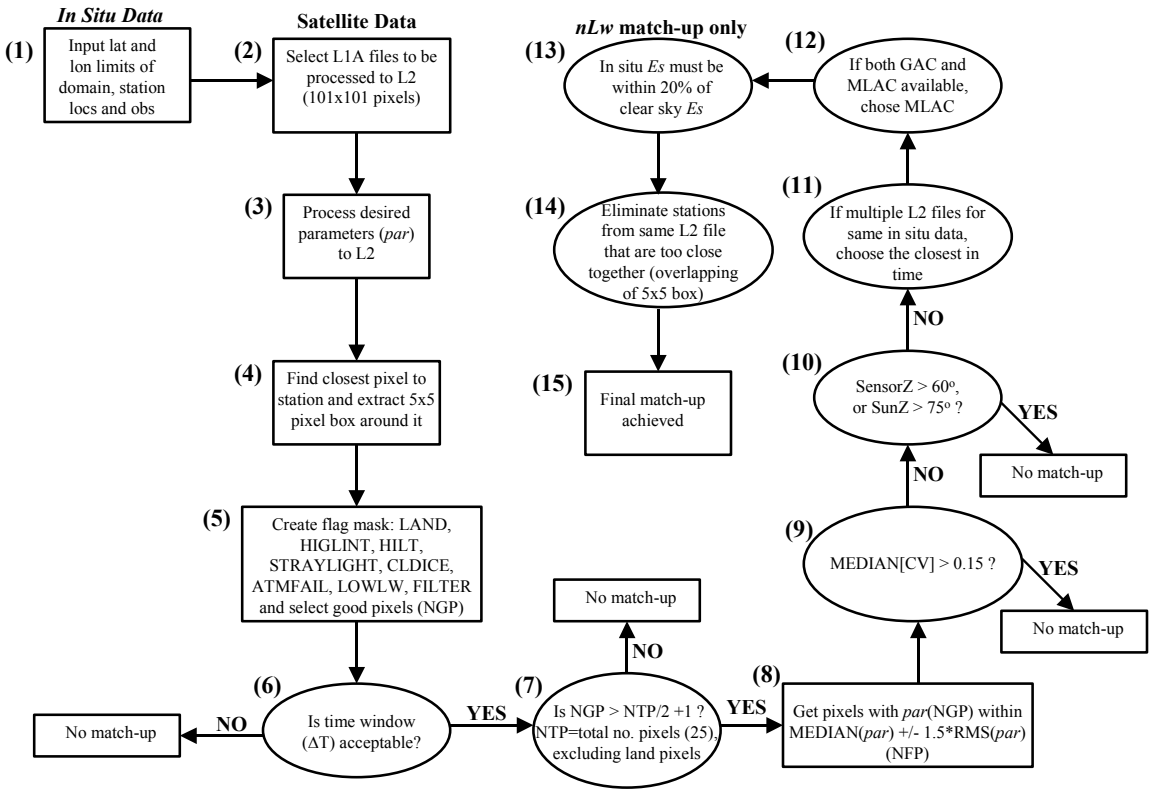

Figure B.1. Flow chart of processing and data filtering sequence (1 through 15) for matching *in situ* records with satellite-derived data.

Figure B.2 shows the water-leaving radiance (*nLw*) match-ups for the SeaWiFS visual bands in Chesapeake Bay following the protocol of Figure B.1. The overall agreement is very good. A statistical summary of the validation analysis is provided as insets on each scatter plot. The data points are color-coded according to the different regional domains defined in Table A.2, e.g., Middle and Lower Bay, and the adjacent shelf (Middle Atlantic Bight, MAB). There were no match-ups in the Upper Bay region. The *in situ* data originated from SeaBASS and was originally provided by Larry Harding's group and collected during Chesapeake Bay Program cruises. The best overall statistical agreement was achieved for the 490, 510, and 555 nm wavelengths (RPD ranging from –5.3% to 4.7%, and APD ranging from 16.0% to 26.8%). However, the other wavelengths are not significantly biased. For instance, for the 670 nm band, the slope, intercept, r^2, RPD, and APD are, respectively, 1.158, -0.024, 0.959, -29.4%, and 33.6%.

Examples of *Chl-a* (Figure B.3) and POC (Figures B.4 and B.5) match-ups for Chesapeake Bay were made using both satellite (POC and *Chl-a*) and in situ reflectances (*Chl-a* only). The OC4v4, GSM01, and GSM01-CB algorithms were used for *Chl-a* and the Stramski-4 and Clark algorithms for POC.

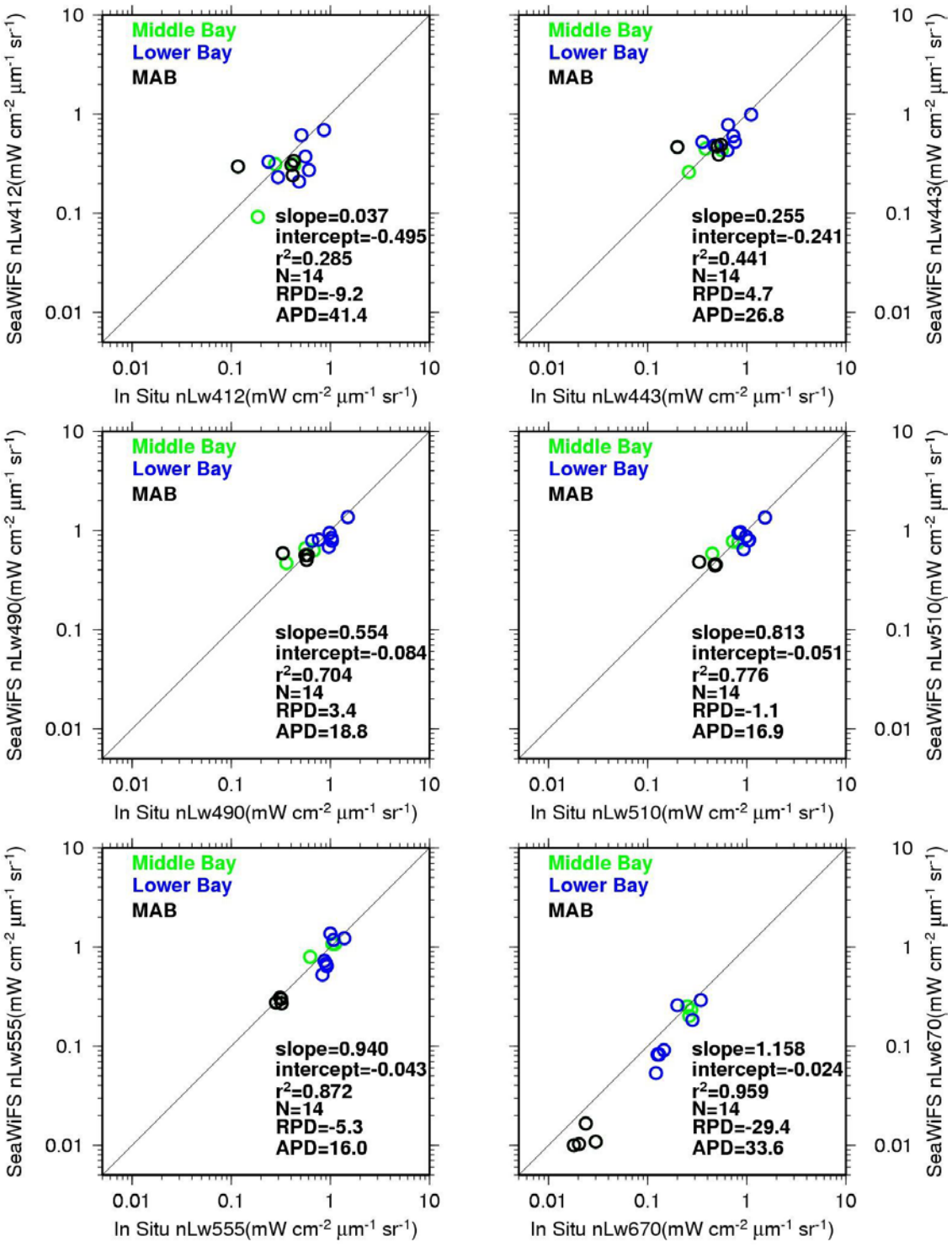

Figure B.2. Scatter plots of *in situ* versus SeaWiFS water-leaving radiances (412, 443, 490, 510, 555, and 670 nm) for Chesapeake Bay. The match-up criteria described in Figure B.1 was applied for the satellite-derived water-leaving radiances. The match-up points are color coded to distinguish the different regional domains.

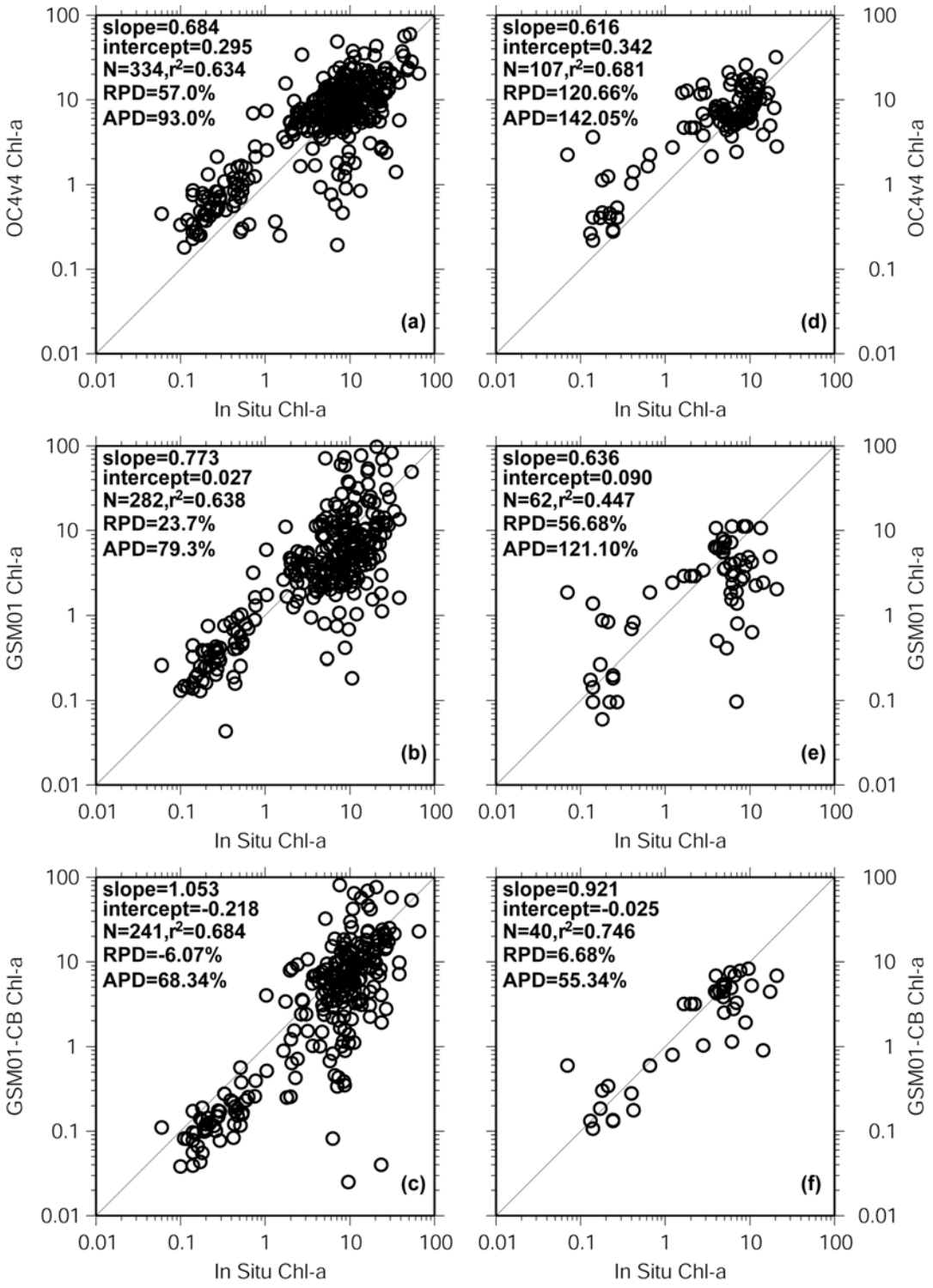

Figure B.3. Scatter plots of *in situ* versus algorithm-derived chlorophyll concentration (mg m^{-3}) for Chesapeake Bay. Three algorithms were used, OC4v4, GSM01, and GSM01-CB, with inputs from both *in situ* (a, b, c) and satellite (d, e, f) reflectances. The match-up criteria described in Figure B.1 was applied for the satellite-derived *Chl-a* but the time window was widened to ±6 hours to increase the number of match-up points.

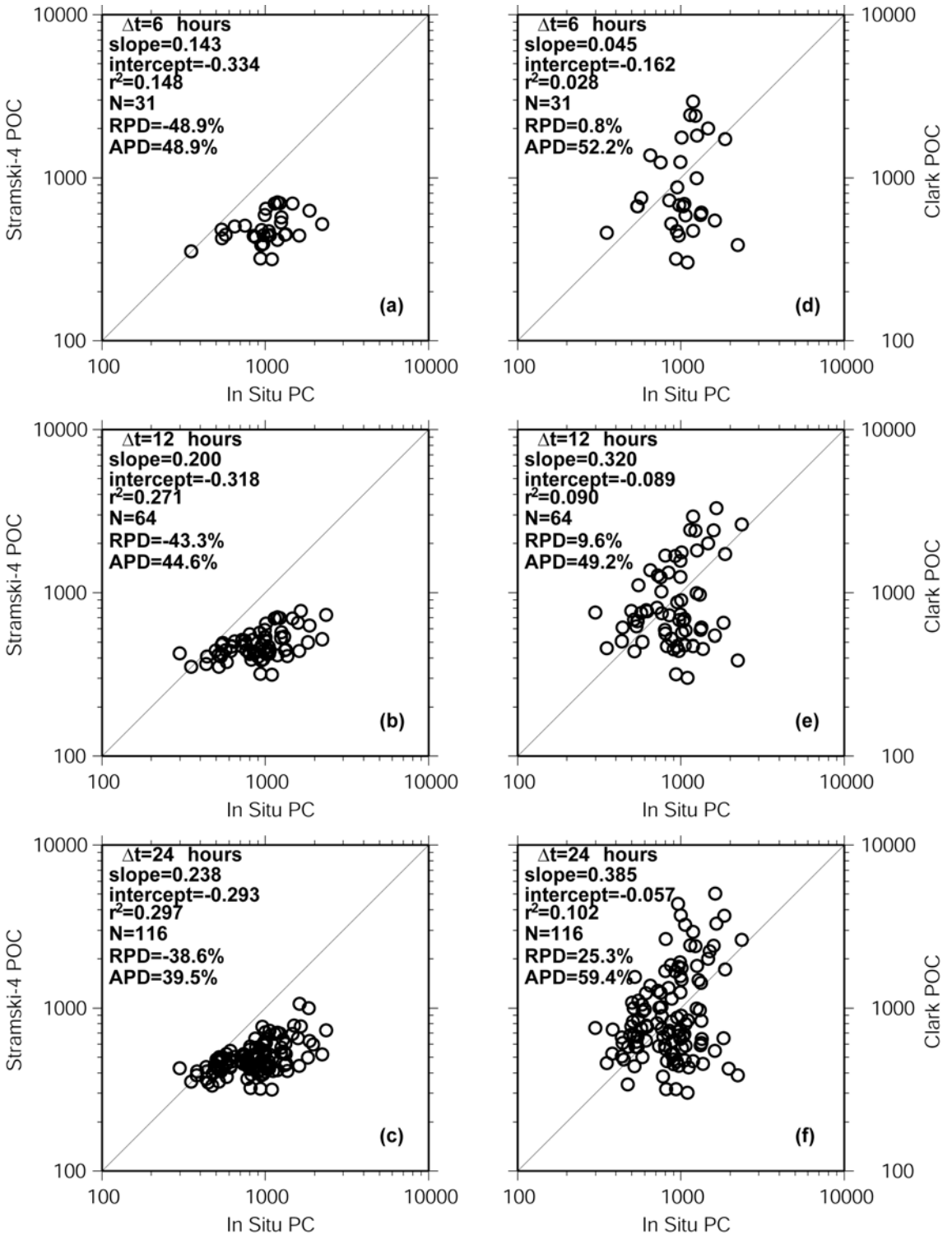

Figure B.4. Scatter plots of *in situ* particulate carbon (PC) versus particulate organic carbon (POC) derived from in-band SeaWiFS reflectances and the Stramski-4 (a, b, and c) and Clark (d, e, and f) POC algorithms. The time windows are 6 hours (±6 hrs), 12 hours (±6 hrs), and 24 hours (±12 hrs). Units of PC and POC are in mg m^{-3}.

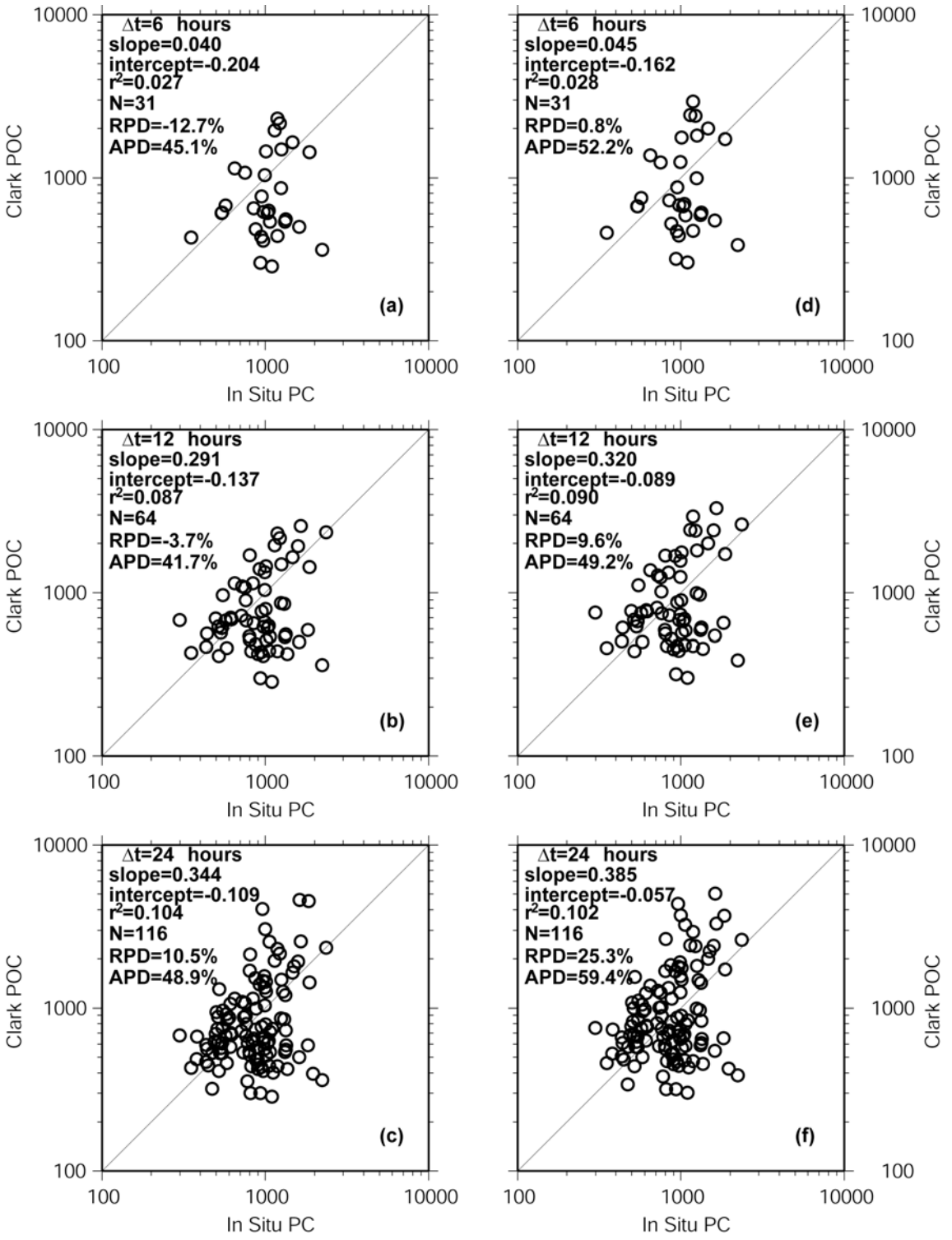

Figure B.5. Scatter plots of *in situ* particulate carbon (PC) versus particulate organic carbon (POC) derived from both full-band (a, b, and c) and in-band (d, e, and f) SeaWiFS reflectances and the Clark POC algorithm. The time windows are 6 hours (±6 hrs), 12 hours (±6 hrs), and 24 hours (±12 hrs). Units of PC and POC are in mg m^{-3}.

References

Atkinson, L.P., G.A. Paffenhofer, and W.M. Dunstan, Chemical and Biological Effect of a Gulf-Stream Intrusion Off St-Augustine, Florida, *Bulletin of Marine Science*, *28* (4), 667-679, 1978.

Austin, R.W., Inherent spectral radiance signatures of the ocean surface, in *Ocean Color Analysis*, pp. 2.1-2.20, Scripps Institute of Oceanography, San Diego, 1974.

Baker, K.S., and R.C. Smith, Bio-Optical Classification and Model of Natural-Waters .2, *Limnology and Oceanography*, *27* (3), 500-509, 1982.

Behrenfeld, M.J., E. Boss, D.A. Siegel, and D.M. Shea, Carbon-based ocean productivity and phytoplankton physiology from space, *Global Biogeochemical Cycles*, *19* (1), 2005.

Behrenfeld, M.J., and P.G. Falkowski, Photosynthetic rates derived from satellite-based chlorophyll concentration, *Limnology and Oceanography*, *42* (1), 1-20, 1997.

Bishop, S.S., J.A. Yoder, and G.A. Paffenhofer, Phytoplankton and Nutrient Variability Along a Cross-Shelf Transect Off Savannah, Georgia, USA, *Estuarine and Coastal Marine Science*, *11* (4), 359-368, 1980.

Blanton, J.O., L.P. Atkinson, C.R. McClain, D.W. Menzel, G.A. Paffenhofer, L.J. Pietrafesa, L.R. Pomeroy, H.L. Wimdom, and J.A. Yoder, A multidisciplinary oceanography program on the southeastern U.S. continental shelf, in *EOS, Trans. Am. Geophys. Union*, pp. 1202-1203, 1984.

Bontempi, P.S., and J.A. Yoder, Spatial variability in SeaWiFS imagery of the South Atlantic bight as evidenced by gradients (fronts) in chlorophyll a and water-leaving radiance, *Deep-Sea Research Part Ii-Topical Studies in Oceanography*, *51* (10-11), 1019-1032, 2004.

Bricaud, A., A. Morel, and L. Prieur, Absorption by dissolved organic matter of the sea (yellow substance) in the UV and visible domains, *Limnol. Oceanogr.*, *26*, 43-53, 1981.

Cai, W.J., Z.H.A. Wang, and Y.C. Wang, The role of marsh-dominated heterotrophic continental margins in transport of CO2 between the atmosphere, the land-sea interface and the ocean, *Geophysical Research Letters*, *30* (16), 2003.

Carder, K.L., F.R. Chen, J.P. Cannizzaro, J.W. Campbell, and B.G. Mitchell, Performance of the MODIS semi-analytical ocean color algorithm for chlorophyll-a, in *Climate Change Processes in the Stratosphere, Earth-Atmosphere-Ocean Systems, and Oceanographic Processes from Satellite Data*, pp. 1152-1159, 2004a.

Carder, K.L., F.R. Chen, J.P. Cannizzaro, S.H. Hawes, and Z.P. Lee, MODIS Ocean Science Team - Algorithm Theoretical Basis Document, pp. 84, College of Marine Sciences, University of Florida, St. Petersburg, 2004b.

Carder, K.L., F.R. Chen, Z.P. Lee, S.K. Hawes, and D. Kamykowski, Semianalytic Moderate-Resolution Imaging Spectrometer algorithms for chlorophyll a and absorption with bio-optical domains based on nitrate-depletion temperatures, *Journal of Geophysical Research-Oceans*, *104* (C3), 5403-5421, 1999.

Dobson, F.W., and S.D. Smith, Bulk Models of Solar-Radiation at Sea, *Quarterly Journal of the Royal Meteorological Society*, *114* (479), 165-182, 1988.

Dunstan, W.M., and L.P. Atkinson, Sources of new nitrogen for the South Atlantic Bight, in *Estuarine Processes*, edited by M. Wiley, pp. 69-78, Academic Press, New York, 1976.

Eppley, R.W., Temperature and phytoplankton growth in the sea, *Fish. Bull.*, *70*, 1063-1085, 1972.

Eppley, R.W., E. Stewart, M.R. Abbott, and U. Heyman, Estimating ocean primary production from satellite chlorophyll. Introduction to regional differences and statistics for the Southern California Bight, *J. Plankton Res.*, *7* (1), 57-70, 1985.

Frouin, R., D.W. Lingner, C. Gautier, K.S. Baker, and R.C. Smith, A Simple Analytical Formula to Compute Clear Sky Total and Photosynthetically Available Solar Irradiance at the Ocean Surface, *Journal of Geophysical Research-Oceans*, *94* (C7), 9731-9742, 1989.

Garver, S.A., and D.A. Siegel, Inherent optical property inversion of ocean color spectra and its biogeochemical interpretation .1. Time series from the Sargasso Sea, *Journal of Geophysical Research-Oceans*, *102* (C8), 18607-18625, 1997.

Gordon, H.R., Ocean color remote sensing: influence of the particle phase function and the solar zenith angle, *EOS Trans. Am. Geophys. Union*, *14*, 1055, 1986.

Gordon, H.R., O.B. Brown, and M.M. Jacobs, Computed Relationships between Inherent and Apparent Optical-Properties of a Flat Homogeneous Ocean, *Applied Optics*, *14* (2), 417-427, 1975.

Green, S.A., and N.V. Blough, Optical absorption and fluorescence properties of chromophoric dissolved organic matter in natural waters, *Limnol. Oceanogr.*, *39*, 1903-1916, 1994.

Haines, E.B., and W.M. Dunstan, Distribution and Relation of Particulate Organic Material and Primary Productivity in Georgia Bight, 1973-1974, *Estuarine and Coastal Marine Science*, *3* (4), 431-441, 1975.

Hanson, R.B., C.Y. Robertson, J.A. Yoder, P.G. Verity, and S.S. Bishop, Nitrogen Recycling in Coastal Waters of Southeastern United-States During Summer 1986, *Journal of Marine Research*, *48* (3), 641-660, 1990.

Hooker, S.B., The calibration and validation of SeaWiFS data, *Progress in Oceanography*, *45*, 427-465, 2000.

Ishizaka, J., Coupling of Coastal Zone Color Scanner Data to a Physical-Biological Model of the Southeastern United-States Continental-Shelf Ecosystem .1. Czcs Data Description and Lagrangian Particle Tracing Experiments, *Journal of Geophysical Research-Oceans*, *95* (C11), 20167-20181, 1990a.

Ishizaka, J., Coupling of Coastal Zone Color Scanner Data to a Physical-Biological Model of the Southeastern United-States Continental-Shelf Ecosystem .2. An Eulerian Model, *Journal of Geophysical Research-Oceans*, *95* (C11), 20183-20199, 1990b.

Ishizaka, J., Coupling of Coastal Zone Color Scanner Data to a Physical-Biological Model of the Southeastern United-States Continental-Shelf Ecosystem .3. Nutrient and Phytoplankton Fluxes and Czcs Data Assimilation, *Journal of Geophysical Research-Oceans*, *95* (C11), 20201-20212, 1990c.

Jerome, J.H., R.P. Bukata, and J.E. Bruton, Utilizing the Components of Vector Irradiance to Estimate the Scalar Irradiance in Natural-Waters, *Applied Optics*, *27* (19), 4012-4018, 1988.

Johannessen, S.C., W.L. Miller, and J.J. Cullen, Calculation of UV attenuation and colored dissolved organic matter absorption spectra from measurements of ocean color, *Journal of Geophysical Research-Oceans*, *108* (C9), 2003.

Kamykowski, D., A Preliminary Biophysical Model of the Relationship between Temperature and Plant Nutrients in the Upper Ocean, *Deep-Sea Research Part a-Oceanographic Research Papers*, *34* (7), 1067-1079, 1987.

Kirk, J.T.O., Volume Scattering Function, Average Cosines, and the Underwater Light-Field, *Limnology and Oceanography*, *36* (3), 455-467, 1991.

Lee, T.N., and L.P. Atkinson, Low frequency current and temperature variability from Gulf Stream frontal eddies and atmospheric forcing along the U. S. outer continental shelf, *J. Geophys. Res.*, *88*, 4541-4567, 1983.

Lee, T.N., L.P. Atkinson, and R. Legeckis, Observations of a Gulf Stream frontal eddy on the Georgia continental shelf, April 1977, *Deep-Sea Research*, *28*, 347-378, 1981.

Lee, Z.P., K.L. Carder, S.H. Hawes, R.G. Steward, T.G. Peacock, and C.O. Davis, A model for interpretation of hyperspectral remote-sensing reflectance, *Appl. Opt.*, *33*, 5721-5732, 1994.

Magnuson, A., J. Harding, Lawrence W., M.E. Mallonee, and J.E. Adolf, Bio-optical model for Chesapeake Bay and the Middle Atlantic Bight, *Estuarine, Coastal and Shelf Science*, *61* (3), 403-424, 2004.

Maritorena, S., D.A. Siegel, and A.R. Peterson, Optimization of a semianalytical ocean color model for global-scale applications, *Applied Optics*, *41* (15), 2705-2714, 2002.

McClain, C.R., and L.P. Atkinson, A Note on the Charleston Gyre, *Journal of Geophysical Research-Oceans*, *90* (NC6), 1857-&, 1985.

McClain, C.R., R. Barnes, R.E. Eplee, B.A. Franz, N.C. Hsu, F.S. Patt, C.M. Pietras, W.D. Robinson, B.D. Schieber, G.M. Schmidt, M. Wang, S. Bailey, and P.J. Werdell, Volume 10, SeaWiFS Postlaunch Calibration and Validation Analyses, Part 2, pp. 57, NASA Goddard Space Flight Center, Greenbelt, 2000.

McClain, C.R., W.E. Esaias, W. Barnes, B. Guenther, D. Endres, S.B. Hooker, G. Mitchell, and R. Barnes, SeaWiFS Calibration and Validation Plan, pp. 1-41, NASA/GSFC, Greenbelt, 1982.

McClain, C.R., J. Ishizaka, and E.E. Hofmann, Estimation of phytoplankton pigment changes on the Southeastern U.S. continental shelf from a sequence of CZCS images and a coupled physical-biological model, *J. Geophys. Res.*, *95* (C11), 20213-20235, 1990.

McClain, C.R., L.J. Pietrafesa, and J.A. Yoder, Observations of Gulf-Stream Induced and Wind-Driven Upwelling in the Georgia Bight Using Ocean Color and Infrared Imagery, *Journal of Geophysical Research-Oceans*, *89* (NC3), 3705-3723, 1984.

McClain, C.R., J.A. Yoder, L.P. Atkinson, J.O. Blanton, T.N. Lee, J.J. Singer, and F. Mullerkarger, Variability of Surface Pigment Concentrations in the South-Atlantic Bight, *Journal of Geophysical Research-Oceans*, *93* (C9), 10675-10697, 1988.

Menzel, D.W., Ocean Processes: U. S. Southeast Continental Shelf. A summary of research conducted in the South Atlantic Bight under the auspices of the U. S. Department of Energy, pp. 112, U. S. Department of Energy, Savannah, 1993.

Morel, A., Optical properties of pure water and pure sea water, in *Optical Aspects of Oceanography*, pp. 1-24, Academic, San Diego, 1974.

Morel, A., Optical Modeling of the Upper Ocean in Relation to Its Biogenous Matter Content (Case-I Waters), *Journal of Geophysical Research-Oceans*, *93* (C9), 10749-10768, 1988.

Morel, A., and J.-F. Berthon, Surface pigments, algal biomass profiles, and potential production of the euphotic layer: Relationships reinvestigated in view of remote-sensing applications, *Limnol. Oceanogr.*, *34* (8), 1545-1562, 1989.

Morel, A., and L. Prieur, Analysis of Variations in Ocean Color, *Limnology and Oceanography*, *22* (4), 709-722, 1977.

O'Reilly, J.E., S. Maritorena, M.C. O'Brien, D.A. Siegel, D. Toole, D. Menzies, R.C. Smith, J.L. Mueller, B.G. Mitchell, M. Kahru, F. Chavez, P. Strutton, G.F. Cota, S.B. Hooker, C.R. McClain, K.L. Carder, F. Müller-Karger, L. Harding, A. Magnuson, D. Phinney, G.F.

Moore, J. Aiken, K.R. Arrigo, R.M. Letelier, and M. Culver, Volume 11, SeaWiFS Postlaunch Calibration and Validation Analyses, Part 3, SeaWiFS Postlaunch Technical Report Series, S. B. Hooker and R. R. Firestone, Editors, NASA/TM-2000-206892, Vol. 11, pp. 49, NASA, Greenbelt, Maryland, 2000.

Pomeroy, L.R., L.P. Atkinson, J.O. Blanton, W.B. Campbell, T.R. Jacobsen, K.H. Kerrick, and A.M. Wood, Microbial Distribution and Abundance in Response to Physical and Biological Processes on the Continental-Shelf of Southeastern USA, *Continental Shelf Research*, *2* (1), 1-20, 1983.

Pope, R.M., and E.S. Fry, Absorption spectrum (380-700 nm) of pure water .2. Integrating cavity measurements, *Applied Optics*, *36* (33), 8710-8723, 1997.

Stramska, M., and D. Stramski, Variability of particulate organic carbon concentration in the north polar Atlantic based on SeaWiFS ocean color observations, *J. Geophys. Res.*, *submitted*, 2005.

Verity, P.G., J.A. Yoder, S.S. Bishop, J.R. Nelson, D.B. Craven, J.O. Blanton, C.Y. Robertson, and C.R. Tronzo, Composition, Productivity and Nutrient Chemistry of a Coastal Ocean Planktonic Food-Web, *Continental Shelf Research*, *13* (7), 741-776, 1993.

Werdell, P.J., and S. Bailey, The SeaWiFS Bio-Optical Archive and Storage System (SeaBASS): Current Architecture and Implementation, pp. 45, NASA Goddard Space Flight Center, Greenbelt, 2002.

Werdell, P.J., S. Bailey, G. Fargion, C. Pietras, K. Knobelspiesse, G. Feldman, and C.R. McClain, Unique data repository facilitates ocean color satellite validation, in *EOS, Transactions, American Geophysical Union*, pp. 379, 385, 2003.

Yoder, J.A., *Environmental control of phytoplankton production on the Southeastern U.S. Continental Shelf, in Oceanography of the southeastern U.S. continental shelf, Coastal and Estuarine Sci.*, American Geophysical Union, Washington, D. C., 1985.

Yoder, J.A., L.P. Atkinson, S.S. Bishop, J.O. Blanton, T.N. Lee, and L.J. Pietrafesa, Phytoplankton dynamics within Gulf Stream intrusions on the southeastern United States continental shelf during summer 1981, *Continental Shelf Research*, *4* (6), 611-635, 1985.

Yoder, J.A., L.P. Atkinson, S.S. Bishop, E.E. Hofmann, and T.N. Lee, Effect of upwelling on phytoplankton productivity on the outer southeastern U.S. continental shelf, *Cont. Shelf Res.*, *1*, 385-404, 1983.

Yoder, J.A., L.P. Atkinson, J.O. Blanton, D.R. Deibel, D.W. Menzel, and G.A. Paffenhofer, Plankton Productivity and the Distribution of Fishes on the Southeastern United-States Continental-Shelf, *Science*, *214* (4518), 352-353, 1981a.

Yoder, J.A., L.P. Atkinson, T.N. Lee, H.H. Kim, and C.R. McClain, Role of Gulf-Stream Frontal Eddies in Forming Phytoplankton Patches on the Outer Southeastern Shelf, *Limnology and Oceanography*, *26* (6), 1103-1110, 1981b.

Yoder, J.A., C.R. McClain, J.O. Blanton, and L.Y. Oey, Spatial Scales in Czcs-Chlorophyll Imagery of the Southeastern United-States Continental-Shelf, *Limnology and Oceanography*, *32* (4), 929-941, 1987.